Communications in Applied Mathematics and Computational Science

GLOBAL PATHS OF TIME-PERIODIC SOLUTIONS OF THE BENJAMIN–ONO EQUATION CONNECTING PAIRS OF TRAVELING WAVES

DAVID M. AMBROSE AND JON WILKENING

vol. 4 no. 1 2009

mathematical sciences publishers

COMM. APP. MATH. AND COMP. SCI.
Vol. 4, No. 1, 2009

GLOBAL PATHS OF TIME-PERIODIC SOLUTIONS OF THE BENJAMIN–ONO EQUATION CONNECTING PAIRS OF TRAVELING WAVES

DAVID M. AMBROSE AND JON WILKENING

We classify all bifurcations from traveling waves to nontrivial time-periodic solutions of the Benjamin–Ono equation that are predicted by linearization. We use a spectrally accurate numerical continuation method to study several paths of nontrivial solutions beyond the realm of linear theory. These paths are found to either reconnect with a different traveling wave or to blow up. In the latter case, as the bifurcation parameter approaches a critical value, the amplitude of the initial condition grows without bound and the period approaches zero. We then prove a theorem that gives the mapping from one bifurcation to its counterpart on the other side of the path and exhibits exact formulas for the time-periodic solutions on this path. The Fourier coefficients of these solutions are power sums of a finite number of particle positions whose elementary symmetric functions execute simple orbits (circles or epicycles) in the unit disk of the complex plane. We also find examples of interior bifurcations from these paths of already nontrivial solutions, but we do not attempt to analyze their analytic structure.

1. Introduction

The Benjamin–Ono equation is a nonlocal, nonlinear dispersive equation intended to describe the propagation of internal waves in a deep, stratified fluid [6; 15; 30]. In spite of nonlocality, it is an integrable Hamiltonian system with meromorphic particle solutions [12; 13], N-soliton solutions [24], and N-phase multiperiodic solutions [32; 16; 26]. A bilinear formalism [32] and a Bäcklund transformation [28; 7; 25] have been found to generate special solutions of the equation, and, in the non-periodic setting of rapidly decaying initial conditions, an inverse scattering transform has been developed [18; 20] that exploits an interesting Lax pair structure

MSC2000: 35Q53, 37G15, 37M20, 65K10.
Keywords: periodic solutions, Benjamin–Ono equation, nonlinear waves, solitons, bifurcation, continuation, exact solution, adjoint equation, spectral method.
This work was supported in part by the National Science Foundation through grant DMS-0926378, and by the Director, Office of Science, Computational and Technology Research, U.S. Department of Energy under contract no. DE-AC02-05CH11231.

in which the solution plays the role of a compatibility condition in a Riemann–Hilbert problem.

It is common practice in numerical analysis to test a numerical method using a problem for which exact solutions can be found. Our initial interest in Benjamin–Ono was to serve as such a test problem. Although many of the tools mentioned above can be used to study time-periodic solutions, they do not generalize to problems such as the vortex sheet with surface tension [4; 3] or the true water wave [31; 19], which are not known to be integrable. Our goal in this paper is to develop tools that *will* generalize to these harder problems and use them to study bifurcation and global reconnection in the space of time-periodic solutions of B–O. Specifically, we employ a variant of the numerical continuation method we introduced in [2] for this purpose, which yields solutions that are accurate enough that we are able to recognize their analytic form.

Because we approached the problem from a completely different viewpoint, our description of these exact solutions is very different from previously known representations of multiperiodic solutions. Rather than solve a system of nonlinear algebraic equations at each x to find $u(x,t)$ as was done in [26], we represent $u(x,t)$ in terms of its Fourier coefficients $c_k(t)$, which turn out to be power sums $c_k = 2[\beta_1^k + \cdots + \beta_N^k]$ of a collection of N particles $\beta_j(t)$ evolving in the unit disk of the complex plane as the zeros of a polynomial $z \mapsto P(z,t)$ whose coefficients execute simple orbits (circles or epicycles in $\mathbb{C}$). The connection between the new representation and previous representations will be explored elsewhere [36].

Many of our findings on the structure of bifurcations and reconnections in the manifold of time-periodic solutions of the Benjamin–Ono equation are likely to hold for other systems as well. One interesting pitfall we have identified by applying our method to an integrable problem is that degenerate bifurcations can exist that are not predicted by counting linearly independent, periodic solutions of the linearization about traveling waves. Although it is possible that such degeneracy is a consequence of the symmetries that make this problem integrable, it is also possible that other problems such as the water wave will also possess degenerate bifurcations that are invisible to a linearized analysis. We have also found that one cannot achieve a complete understanding of these manifolds of time-periodic solutions by holding, for example, the mean constant and varying only one parameter. In some of the simulations where we hold the mean fixed, the solution (that is, the L^2 norm of the initial condition) blows up as the parameter approaches a critical value rather than reconnecting with another traveling wave. However, if the mean is simultaneously varied, it is always possible to reconnect. Thus, although numerical continuation with more than one parameter is difficult, it will likely be necessary to explore multidimensional parameter spaces to achieve a thorough understanding of time-periodic solutions of other problems.

On the numerical side, we believe our use of certain Fourier modes of the initial conditions as bifurcation parameters will prove useful in many other problems beyond Benjamin–Ono. We also wish to advocate the use of variational calculus and optimal control for the purpose of finding time-periodic solutions (or solving other two-point boundary value problems). For ODE, a competing method known as orthogonal collocation (for example, as implemented in AUTO [17]) has proved to be a very powerful technique for solving boundary value problems. This approach becomes quite expensive when the dimension of the system increases, and is therefore less competitive for PDE than it is for ODE. For PDE, many authors do not attempt to find exact periodic solutions, and instead point out that typical solutions of certain equations do tend to pass near their initial states at a later time [11]. If true periodic solutions are sought, a more common approach has been to either iterate on a Poincaré map and use stability of the orbit to find time-periodic solutions [10], or use a shooting method [33; 35] to find a fixed point of the Poincaré map.

In a shooting method, we define a functional $F(u_0, T) = [u(\cdot\,, T) - u_0]$ that maps initial conditions and a supposed period to the deviation from periodicity. The equation $F = 0$ is then solved by Newton's method, where the Jacobian $J = DF$ is either computed using finite differences [34] or by solving the variational equation repeatedly to compute each column of J. We have found that it is much more efficient (by a factor of the number of columns of J) to instead minimize the scalar functional $G = \frac{1}{2}\|F\|^2$ via a quasi-Newton method in which the gradient DG is computed by solving an adjoint PDE.

Bristeau et. al. [8] developed a similar approach for linear (but two- or three-dimensional) scattering problems. Three-dimensional problems are intractable by the standard shooting approach as J could easily have 10^5 columns. However, the gradient of G can be computed by solving a single adjoint PDE. The success of the method then boils down to a question of the number of iterations required for the minimization algorithm to converge. For linear problems, Bristeau et. al. have had success using conjugate gradients to minimize G. We find that BFGS [9] works very well for nonlinear problems like the Benjamin–Ono equation and the vortex sheet with surface tension [3].

To find nontrivial time-periodic solutions in the present work, we use a symmetric variant of the algorithm described in [2]. Although the original method works well, we use the symmetric variant for the simulations in this paper because evolving to $T/2$ requires half the time-steps and yields more accurate answers (as there is less time for numerical round-off error to corrupt the calculation). Moreover, the number of degrees of freedom in the search space of initial conditions is also cut in half and the condition number of the problem improves when we eliminate phase shift degrees of freedom via symmetry rather than including them in the penalty function described in Section 3.1. Although we do not make use of it, there is a procedure known as the Meyer–Marsden–Weinstein reduction [27; 23] that allows one to reduce the dimension of a symplectic manifold on which a group acts symplectically. This allows one to eliminate actions of the group (for example, translations) from the phase space. Equilibria and periodic solutions of the reduced Hamiltonian system correspond to (families of) relative equilibria and relative periodic solutions [39] of the original system.

This paper is organized as follows. In Section 2, we discuss stationary, traveling and particle solutions of B-O, linearize about traveling waves, and classify all bifurcations predicted by linear theory from traveling waves to nontrivial time-periodic solutions. Some of the more technical material from this section is given in Appendix A. In Section 3, we present a collection of numerical experiments using our continuation method to follow several paths of nontrivial solutions beyond the realm of linear theory in order to formulate a theorem that gives the global mapping from one traveling wave bifurcation to its counterpart on the other side of the path. In Section 4, we study the behavior of the Fourier modes of the time-periodic solutions found in Section 3 and state a theorem about the exact form of these solutions, which is proved in Appendix B. Finally, in Section 5, we discuss interior bifurcations from these paths of already nontrivial solutions to still more complicated solutions. Although the existence of such a hierarchy of solutions was already known [32], bifurcation between various levels of the hierarchy has not previously been discussed.

2. Bifurcation from traveling waves

In this section, we study the linearization of the Benjamin–Ono equation about stationary solutions and traveling waves by solving an infinite dimensional eigenvalue problem in closed form. Each eigenvector corresponds to a time-periodic solution of the linearized equation. The traveling case is reduced to the stationary case by requiring that the period of the perturbation (with a suitable spatial phase shift) coincide with the period of the traveling wave. The main goal of this section is to devise a classification scheme of the bifurcations from traveling waves so that in later sections we can describe which (local) bifurcations are connected together by a global path of nontrivial time-periodic solutions.

2.1. ***Stationary, traveling and particle solutions.*** We consider the Benjamin–Ono equation on the periodic interval $\mathbb{R}/2\pi\mathbb{Z}$, namely,

$$u_t = Hu_{xx} - uu_x. \tag{1}$$

Here H is the Hilbert transform, which has the symbol $\hat{H}(k) = -i\,\mathrm{sgn}(k)$. The Benjamin–Ono equation possesses solutions [12; 2] of the form

$$u(x,t) = \alpha_0 + \sum_{l=1}^{N} \phi(x; \beta_l(t)), \tag{2}$$

where α_0 is the mean, $\beta_1(t), \dots, \beta_N(t)$ are the trajectories of N particles evolving in the unit disk Δ of the complex plane and governed by the ODE

$$\dot{\beta}_l = \sum_{\substack{m=1\\ m\neq l}}^{N} \frac{-2i\beta_l^2}{\beta_l - \beta_m} + \sum_{m=1}^{N} \frac{2i\beta_l^2}{\beta_l - \bar{\beta}_m^{-1}} + i(2N-1-\alpha_0)\beta_l \quad (1 \le l \le N), \tag{3}$$

and $\phi(x;\beta)$ is the function with Fourier representation

$$\hat{\phi}(k;\beta) = \left\{ \begin{array}{ll} 0, & k=0 \\ 2\beta^k, & k>0 \\ 2\bar{\beta}^{|k|}, & k<0 \end{array} \right\}, \qquad \beta \in \Delta = \{z : |z| < 1\}. \tag{4}$$

The function $\phi(x;\beta)$ has a peak centered at $x = \arg(\bar{\beta})$ with amplitude growing to infinity as $|\beta|$ approaches 1. The N-hump traveling waves (with a spatial period of $2\pi/N$) are a special case of the particle solutions given by (2) and (3):

$$\begin{gathered} u_{\text{trav}}(x,t;\alpha_0,N,\beta) = \alpha_0 + \sum_{l=1}^{N} \phi(x;\beta_l(t)), \quad \beta_l(t) = \sqrt[N]{\beta}e^{-ict}, \\ c = \alpha_0 - N\alpha(\beta). \end{gathered} \tag{5}$$

Each β_l is assigned a distinct N-th root of β and $\alpha(\beta)$ is the mean of the one-hump stationary solution, namely,

$$\alpha(\beta) = \frac{1-3|\beta|^2}{1-|\beta|^2}, \quad |\beta|^2 = \frac{1-\alpha(\beta)}{3-\alpha(\beta)}. \tag{6}$$

The solution (5) moves to the right when $c > 0$. Indeed, it may also be written

$$u_{\text{trav}}(x,t;\alpha_0,N,\beta) = u_{\text{stat}}(x-ct;N,\beta) + c, \tag{7}$$

where u_{stat} is the N-hump stationary solution

$$u_{\text{stat}}(x;N,\beta) = N\alpha(\beta) + \sum_{\{\gamma : \gamma^N = \beta\}} \phi(x;\gamma) \; = \; N\alpha(\beta) + N\phi(Nx;\beta). \tag{8}$$

The Fourier representation of u_{stat} is

$$\hat{u}_{\text{stat}}(k;N,\beta) = \begin{cases} N\alpha(\beta), & k=0, \\ 2N\beta^{k/N}, & k \in N\mathbb{Z},\ k>0, \\ 2N\bar{\beta}^{|k|/N}, & k \in N\mathbb{Z},\ k<0, \\ 0, & \text{otherwise}. \end{cases} \tag{9}$$

Amick and Toland have shown [5] that all traveling waves of the Benjamin–Ono equation have the form (7); see also [36].

2.2. ***Linearization about stationary solutions.*** Let $u(x) = u_{\text{stat}}(x; N, \beta)$ be an N-hump stationary solution. In [2], we solved the linearization of (1) about u, namely,

$$v_t = Hv_{xx} - (uv)_x = iBAv, \quad A = H\partial_x - u, \quad B = \frac{1}{i}\partial_x, \tag{10}$$

by substituting the expression $v(x,t) = \text{Re}\{Cz(x)e^{i\omega t}\}$ into (10) and solving the eigenvalue problem

$$BAz = \omega z \tag{11}$$

in closed form. Specifically, we showed that the eigenvalues $\omega_{N,n}$ are given by

$$\omega_{N,n} = \left\{ \begin{array}{ll} -\omega_{N,-n}, & n < 0 \\ 0, & n = 0 \\ (n)(N-n), & 1 \le n \le N-1 \\ (n+1-N)\big(n+1+N(1-\alpha(\beta))\big), & n \ge N \end{array} \right\} \tag{12}$$

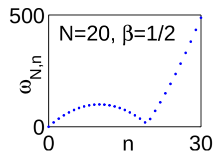

The zero eigenvalue $\omega_{N,0} = 0$ has geometric multiplicity two and algebraic multiplicity three. The eigenfunctions in the kernel of BA are

$$z_{N,0}^{(1,0)}(x) = -\frac{\partial}{\partial x}u_{\text{stat}}(x; N, \beta), \quad z_{N,0}^{(2)}(x) = \frac{\partial}{\partial|\beta|}u_{\text{stat}}(x; N, \beta), \tag{13}$$

which correspond to changing the phase or amplitude of β in the underlying stationary solution. There is also a Jordan chain [37] of length two associated with $z_{N,0}^{(1,0)}(x)$, namely,

$$z_{N,0}^{(1,1)}(x) = 1, \quad \big(iBAz_{N,0}^{(1,1)} = z_{N,0}^{(1,0)}\big), \tag{14}$$

which corresponds to the fact that adding a constant to a stationary solution causes it to travel. The fact that all the eigenvalues $i\omega_{N,n}$ in the linearization (10) are purely imaginary is a consequence of the Hamiltonian structure [13] of the Benjamin–Ono equation. For non-Hamiltonian systems, one does not generally expect to find time-periodic perturbations of traveling waves (as periodic solutions of the linearized problem may not even exist).

The eigenfunctions $z_{N,n}(x)$ corresponding to positive eigenvalues $\omega_{N,n}$ (with $n \ge 1$) have the Fourier representation

$$\hat{z}_{N,n}(k)\Big|_{k=n+jN} = \left\{ \begin{array}{ll} \left(1+\dfrac{N(|j|-1)}{N-n}\right)\bar{\beta}^{|j|-1}, & j<0 \\ C\left(1+\dfrac{Nj}{n}\right)\beta^{j+1}, & j\geq 0 \end{array} \right\}$$
$$\left(1 \leq n \leq N-1, \quad C = \frac{-nN}{(N-n)\big[n+(N-n)|\beta|^2\big]}\right), \tag{15}$$
$$\hat{z}_{N,n}(k)\Big|_{k=n+1-N+jN} = \left\{ \begin{array}{ll} 0, & j<0 \\ \dfrac{-\bar{\beta}}{(1-|\beta|^2)^2}\left[1-\left(1-\dfrac{N}{n+1}\right)|\beta|^2\right], & j=0 \\ \left(1+\dfrac{N(j-1)}{n+1}\right)\beta^{j-1}, & j>0 \end{array} \right\} \quad (n \geq N),$$

with all other Fourier coefficients equal to zero. The eigenfunctions corresponding to negative eigenvalues $\omega_{N,n}$ (with $n \leq -1$) satisfy $z_{N,n}(x) = \overline{z_{N,-n}(x)}$, so the Fourier coefficients appear in reverse order, conjugated. For $1 \leq n \leq N-1$, any linear combination of $z_{N,n}(x)$ and $z_{N,N-n}(x)$ is also an eigenfunction; however, the choices here seem most natural as they simultaneously diagonalize the shift operator (discussed below) and yield directions along which nontrivial solutions exist beyond the linearization. Said differently, we have listed the first $N-1$ positive eigenvalues $\omega_{N,n}$ in an unusual order (rather than enumerating them monotonically and coalescing multiple eigenvalues) because this is the order that leads to the simplest description of the global paths of nontrivial solutions connecting these traveling waves.

2.3. ***Classification of bifurcations from traveling waves.*** Time-periodic solutions of the Benjamin–Ono equation with period T have initial conditions that satisfy $F(u_0, T) = 0$, where $F : H^1 \times \mathbb{R} \to H^1$ is given by

$$F(u_0, T) = u(\,\cdot\,, T) - u_0, \quad u_t = Hu_{xx} - uu_x, \quad u(\,\cdot\,, 0) = u_0. \tag{16}$$

First, we linearize F about an N-hump stationary solution $u_0(x) = u_{\text{stat}}(x; N, \beta)$. The Fréchet derivative $DF = (D_1F, D_2F) : H^1 \times \mathbb{R} \to H^1$ yields directional derivatives

$$\begin{aligned} D_1F(u_0, T)v_0 &= \frac{\partial}{\partial\varepsilon}\Big|_{\varepsilon=0} F(u_0+\varepsilon v_0, T) = v(\,\cdot\,, T) - v_0 = \big[e^{iBAT} - I\big]\, v_0, \\ D_2F(u_0, T)\tau &= \frac{\partial}{\partial\varepsilon}\Big|_{\varepsilon=0} F(u_0, T+\varepsilon\tau) = 0. \end{aligned} \tag{17}$$

Note that $v_0 \in \ker D_1F(u, T)$ if and only if the solution $v(x, t)$ of the linearized problem is periodic with period T. As a result, a basis for the kernel $\mathcal{N} = \ker DF(u_0, T)$

consists of $(0; 1)$ together with all pairs $(v_0; 0)$ of the form

$$v_0(x) = \mathrm{Re}\{z_{N,n}(x)\} \quad \text{or} \quad v_0(x) = \mathrm{Im}\{z_{N,n}(x)\}, \tag{18}$$

where n ranges over all integers such that

$$\omega_{N,n} T \in 2\pi\mathbb{Z}, \tag{19}$$

with N and β (in the formula (12) for $\omega_{N,n}$) held fixed. The corresponding periodic solutions of the linearized problem are

$$v(x,t) = \mathrm{Re}\{z_{N,n}(x)e^{i\omega_{N,n}t}\} \quad \text{or} \quad v(x,t) = \mathrm{Im}\{z_{N,n}(x)e^{i\omega_{N,n}t}\}. \tag{20}$$

Negative values of n have already been accounted for in (18) and (20) using $z_{N,-n}(x) = \overline{z_{N,n}(x)}$, and the $n = 0$ case always yields two vectors in the kernel, namely, those in (13). These directions do not cause bifurcations as they lead to other stationary solutions.

Next we wish to linearize F about an arbitrary traveling wave. Suppose $u(x) = u_{\mathrm{stat}}(x; N, \beta)$ is an N-hump stationary solution and $U(x,t) = u(x - ct) + c$ is a traveling wave. Then the solutions v and V of the linearizations about u and U, respectively, satisfy $V(x,t) = v(x - ct, t)$. Note also that

$$F(U_0, T) = 0 \quad \text{if and only if} \quad cT = \frac{2\pi\nu}{N} \quad \text{for some } \nu \in \mathbb{Z}, \tag{21}$$

where $U_0(x) = U(x,0) = u(x) + c$. Note that ν is the number of times the traveling wave turns over itself in one period. Assuming (21) holds, we set $\theta = 2\pi\nu/N$ and compute

$$\begin{aligned} [D_1F(U_0,T)v_0](x) &= v(x - cT, T) - v_0(x) = [(S_\theta e^{iBAT} - I)v_0](x), \\ [D_2F(U_0,T)\tau](x) &= U_t(x,T)\tau = -cu_x(x - cT)\tau = -cu_x(x)\tau, \end{aligned} \tag{22}$$

where v solves (10) and the shift operator S_θ is defined via

$$S_\theta z(x) = z(x - \theta), \quad \hat{S}_{\theta,kl} = e^{-ik\theta}\delta_{kl}. \tag{23}$$

One element of $\mathcal{N} = \ker DF(U_0, T)$ arises from (14), which gives

$$e^{iBAt}1 = 1 - tu_x \quad \Rightarrow \quad D_1F(U_0,T)(-c/T) + D_2F(U_0,T)1 = 0,$$

and implies $(-c/T; 1) \in \mathcal{N}$. This just means that we can change the period T by a small amount τ by adding the constant $-(c/T)\tau$ to U_0 (this also follows from the condition (21) that $cT = \theta = \text{const}$). If we wish to change the period without changing the mean, we need to simultaneously adjust $|\beta|$ in the underlying stationary solution $u(x) = u_{\mathrm{stat}}(x; N, \beta)$. The other elements of $\mathcal{N}$ are of the form $(v_0; 0)$ with

$$v_0(x) = \mathrm{Re}\{z_{N,n}(x)\} \quad \text{or} \quad v_0(x) = \mathrm{Im}\{z_{N,n}(x)\}. \tag{24}$$

The admissible values of n here are found using (22) together with

$$S_\theta e^{iBAT} z_{N,n} = e^{i(\omega_{N,n}T-\theta k_{N,n})} z_{N,n}, \quad \theta = \frac{2\pi\nu}{N}, \tag{25}$$

where $k_{N,n}$ is the stride offset of the non-zero Fourier coefficients of $z_{N,n}$, i.e.,

$$\hat{z}_{N,n}(k) \neq 0 \quad \Rightarrow \quad k - k_{N,n} \in N\mathbb{Z}. \tag{26}$$

Thus, instead of (19), n ranges over all integers such that

$$\omega_{N,n}T \in 2\pi\left(\frac{\nu k_{N,n}}{N} + \mathbb{Z}\right), \quad k_{N,n} = \begin{cases} -k_{N,-n}, & n < 0, \\ 0, & n = 0, \\ n, & 1 \le n \le N-1, \\ \operatorname{mod}(n+1, N), & n \ge N. \end{cases} \tag{27}$$

As before, negative values of n need not be considered once we take real and imaginary parts in (24), and the $n = 0$ case always gives the two vectors $(z_{N,0}^{(1,0)}; 0)$ and $(z_{N,0}^{(2)}; 0)$ in $\mathcal{N}$, which lead to other traveling waves rather than bifurcations to nontrivial solutions.

Our numerical experiments have led us to the following conjecture, which we prove as part of Theorem 3 in Section 4:

Conjecture 1. For every $\beta \in \Delta$ and $(N, \nu, n, m) \in \mathbb{Z}^4$ satisfying

$$N \ge 1, \quad \nu \in \mathbb{Z}, \quad n \ge 1, \quad m \ge 1, \quad m \in \nu k_{N,n} + N\mathbb{Z}, \tag{28}$$

there is a four parameter sheet of nontrivial time-periodic solutions bifurcating from the N-hump traveling wave with speed index ν, $(cT = 2\pi\nu/N)$, bifurcation index n, and oscillation index m, $(\omega_{N,n}T = 2\pi m/N)$. The phase and amplitude of the traveling wave are determined by β.

The main content of this conjecture is that we do not have to consider linear combinations of the $z_{N,n}$ with different values of n to find periodic solutions of the nonlinear problem — this basis is already "diagonal" with respect to these bifurcations. This is true in spite of a small divisor problem preventing $DF(U_0, T)$ from being Fredholm. The decision to number the first $N - 1$ eigenvalues $\omega_{N,n}$ nonmonotonically in (12) and to simultaneously diagonalize the shift operator S_θ when choosing eigenvectors $z_{N,n}$ in (15) was essential to make this work. Formulas relating the period, T, the mean, α_0, and the decay parameter, $|\beta|$, for each of these bifurcations are given in Appendix A along with a list of bifurcation rules governing "legal" values of the mean.

A canonical way to generate one of these bifurcations is to take β real and perturb the initial condition in the direction $v_0(x) = \operatorname{Re}\{z_{N,n}(x)\}$. This leads to nontrivial solutions with even symmetry at $t = 0$. Perturbation in the $\operatorname{Im}\{z_{N,n}(x)\}$ direction yields the same set of nontrivial solutions, but with a spatial and temporal phase shift:

$$\mathrm{Im}\{z_{N,n}(x-ct)e^{i\omega t}\} = \mathrm{Re}\Big\{z_{N,n}\Big(\Big(x-\frac{c\pi}{2\omega}\Big)-c\Big(t-\frac{\pi}{2\omega}\Big)\Big)e^{i\omega(t-(\pi/2\omega))}\Big\}, \quad (29)$$

where $\omega=\omega_{N,n}$. The manifold of nontrivial solutions is four dimensional with two essential parameters (for example, the mean α_0 and a parameter governing the distance from the traveling wave) and two inessential parameters (the spatial and temporal phase). In our numerical studies, we use the real part of a Fourier coefficient c_k of the initial condition (with k such that $\hat{z}_{N,n}(k)\neq 0$) for the second essential bifurcation parameter. When we discuss exact solutions in Section 4, a different parameter will be used.

We remark that this enumeration of bifurcations accounts for all time-periodic solutions of the linearization about traveling waves; therefore, the heuristic that each bifurcation of the nonlinear problem gives rise to a linearly independent vector in the kernel $\mathcal{N}$ of the linearized problem suggests that we have found all bifurcations from traveling waves. Interestingly, this turns out not to be the case; the interior bifurcations we discuss in Section 5 can occur at the endpoints of the path, allowing for degenerate bifurcations directly from traveling waves to higher levels in the infinite hierarchy of time-periodic solutions. Only the transition from the first level of the hierarchy to the second is "visible" to a linearized analysis about traveling waves. The other transitions become linearly dependent on these in the limit as the traveling wave is approached; they will be analyzed in [36].

3. Numerical experiments

In this section we present a collection of numerical experiments in which we start with a given bifurcation (N,ν,n,m,β) and use a symmetric variant of the method we described in [2] for finding periodic solutions of nonlinear PDE to continue these solutions until another traveling wave is found, or until the solution blows up as the bifurcation parameter approaches a critical value. We determine the bifurcation indices (N',ν',n',m') at the other end of the path of nontrivial solutions by fitting the data to the formulas of the previous section. By trial and error, we are then able to guess a formula relating (N',ν',n',m') to (N,ν,n,m) that we use in Section 4 to construct exact solutions.

3.1. ***Numerical method.*** As mentioned in Section 2.3, a natural choice of spatial and temporal phase can be achieved by choosing the parameter β of the traveling wave to be real and perturbing the initial condition in the direction $v_0(x)=\mathrm{Re}\{z_{N,n}(x)\}$. For reasons of efficiency and accuracy (explained in the introduction), we now restrict our search for time-periodic solutions of (1) to functions $u(x,t)$ that possess even spatial symmetry at $t=0$. If we succeed in finding solutions with this symmetry, then they — together with their phase-shifted counterparts analogous to (29) — span the nullspace $\mathcal{N} = \ker DF(U_0, T)$ in the limit that the perturbation goes to zero. Thus, we do not expect symmetry breaking bifurcations from traveling waves that cannot be phase shifted to have even symmetry at $t = 0$.

The Benjamin–Ono equation has the property that if $u(x,t)$ is a solution of (1), then so is $U(x,t) = u(-x,-t)$. As a result, if u is a solution such that $u(x, T/2) = U(x, -T/2)$, then $u(x,T) = U(x,0)$, i.e., u is time-periodic if the initial condition has even symmetry. Thus, we seek initial conditions u_0 with even symmetry and a period T to minimize the functional

$$G_{\text{tot}}(u_0, T) = G(u_0, T) + G_{\text{penalty}}(u_0, T), \tag{30}$$

where

$$G(u_0, T) = \frac{1}{2}\int_0^{2\pi} [u(x, T/2) - u(2\pi - x, T/2)]^2\, dx, \tag{31}$$

and $G_{\text{penalty}}(u_0, T)$ is a non-negative penalty function to impose the mean and set the bifurcation parameter. To compute the gradient of G with respect to variation of the initial conditions, we use

$$\left.\frac{d}{d\varepsilon}\right|_{\varepsilon=0} G(u_0 + \varepsilon v_0, T) = \int_0^{2\pi} \frac{\delta G}{\delta u_0}(x) v_0(x)\, dx, \tag{32}$$

where the variational derivative

$$\frac{\delta G}{\delta u_0}(x) = 2w(x, T/2), \qquad w_0(x) = u(x, T/2) - u(2\pi - x, T/2) \tag{33}$$

is found by solving the following adjoint equation from $s = 0$ to $s = T/2$:

$$w_s(x,s) = -H w_{xx}(x,s) + u(x, T/2 - s) w_x(x,s), \qquad w(\,\cdot\,, 0) = w_0. \tag{34}$$

Since v_0 is assumed symmetric in this formulation, (33) is equivalent to

$$\frac{\delta G}{\delta u_0}(x) = w(x, T/2) + w(2\pi - x, T/2). \tag{35}$$

The Benjamin–Ono and adjoint equations are solved using a pseudo-spectral collocation method employing a fourth order semi-implicit additive Runge–Kutta method [14; 21; 38] to advance the solution in time. The BFGS method [9; 29] is then used to minimize G_{tot} (varying the period and the Fourier coefficients of the initial conditions). We use the penalty function

$$G_{\text{penalty}}(u_0, T) = 1/2([a_0(0) - \alpha_0]^2 + [a_K(0) - \rho]^2) \tag{36}$$

to specify the mean α_0 and the real part ρ of the K-th Fourier coefficient of the initial condition

$$u_0(x) = \sum_{k=-M/2+1}^{M/2} c_k(0)e^{ikx}, \quad c_k(t) = a_k(t) + ib_k(t). \tag{37}$$

The parameters α_0 and ρ serve as the bifurcation parameters while the phases are determined by requiring that the solution have even symmetry at $t = 0$. We generally choose K to be the first $k \geq 1$ such that $\hat{z}_{N,n}(k) \neq 0$.

Our continuation method consists of three stages. First, we choose a traveling wave and a set of bifurcation indices to begin the path of nontrivial solutions. We also choose a direction in which to vary the bifurcation parameter ρ and the mean α_0. In most of our numerical experiments, we hold α_0 fixed; however, in the example of Figure 6 below, we vary ρ and α_0 simultaneously. The traveling wave serves as the zeroth point on the path. The initial guess for the first point on the path is obtained by perturbing the initial condition of the traveling wave in the direction $\mathrm{Re}\{z_{N,n}(x)\}$. We use the period T given in (A.1) in Appendix A as a starting guess. We then use the minimization algorithm to descend from the starting guess predicted by linear theory to an actual time-periodic solution. The second stage of the continuation algorithm consists of varying ρ (and possibly α_0), using linear extrapolation for the starting guess (for u_0 and T) of the next solution, and then minimizing G_{tot} to find an actual time-periodic solution with these values of ρ and α_0. If the initial value of G_{tot} from the extrapolation step is too large, we discard the step and try again with a smaller change in ρ and α_0. The final stage of the algorithm consists of identifying the reconnection on the other side of the path. We do this by blindly overshooting the target values of ρ and α_0 (which we do not know in advance). Invariably, the algorithm will lock onto a family of traveling waves once we reach the end of the path of nontrivial solutions. We look at the Fourier coefficients of the last nontrivial solution before the traveling waves are reached and match them with the formulas for $\hat{z}_{N',n'}(k)$ to determine the correct bifurcation indices on this side of the path. (A prime indicates indices for the bifurcation at the other end of the path.) We then recompute the last several solutions on the path of nontrivial solutions with appropriate values of ρ and α_0 to arrive exactly at the traveling wave on the last iteration. We sometimes change K in (36) to compute this reconnection to avoid $\hat{z}_{N',n'}(K) = 0$.

The running time of our algorithm (on a 2.4 GHz desktop machine) varies from a few hours to compute one of the paths labeled *a*–*l* in (38)–(41) below, to a few days to compute a path in which the solution blows up, such as the one shown in Figure 5 (page 196). We always refine the mesh and timestep enough so that the solutions are essentially exact (with $G_{\text{tot}} \leq 10^{-26}$ in the easy cases and 10^{-20} in the hard cases).

3.2. ***Global paths of nontrivial solutions.*** We now investigate the global behavior of nontrivial solutions that bifurcate from arbitrary stationary or traveling waves. We find that these nontrivial solutions act as rungs in a ladder, connecting stationary and traveling solutions with different speeds and wavelengths by creating or annihilating oscillatory humps that grow or shrink in amplitude until they become part of the stationary or traveling wave on the other side of the rung. In some cases, rather than reconnecting with another traveling wave, the solution blows up (the L^2 norm of the initial condition grows without bound) as the bifurcation parameter ρ approaches a critical value. However, even in these cases a reconnection with another traveling wave does occur if, in addition to ρ, we vary the mean, α_0, appropriately.

Recall from Section 2.3 that we can enumerate all such bifurcations by specifying a complex parameter β in the unit disk Δ along with four integers (N, ν, n, m) satisfying (28), and in most cases we can solve for $|\beta|$ in terms of the mean, α_0, using (A.4) in Appendix A. In [2], we presented a detailed study of the solutions on the path connecting a one-hump stationary solution to a two-hump traveling wave moving left. We denote this path by

$$a: \quad (1, 0, 1, 1) \quad \longleftrightarrow \quad (2, -1, 1, 1), \tag{38}$$

where the label a refers to the bifurcation diagram in Figure 1.

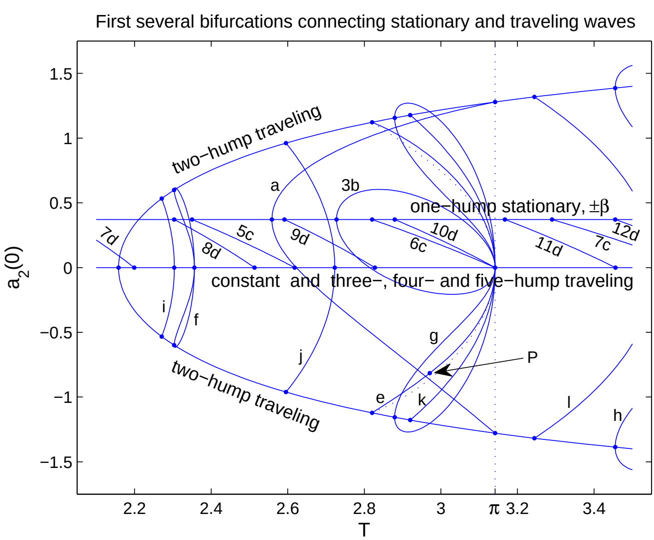

Figure 1. Paths of nontrivial solutions listed in (38)–(41). The second Fourier mode of the eigenvector $z_{N,n}(x)$ in the linearization is nonzero for the pitchfork bifurcations and is zero for the one-sided, oblique-angle bifurcations. The point labeled P corresponds to the solution in Figure 3 below.

We have also computed the next several bifurcations ($n = 2, 3, 4$) from the one-hump stationary solution and found that they connect up with a traveling wave with $N' = n + 1$ humps moving left with speed index $\nu' = -1$, where we denote the bifurcation on the other side of the path by (N', ν', n', m'). By comparing the Fourier coefficients of the last few nontrivial solutions on these paths to those of the linearization about the N'-hump traveling wave, we determined that the bifurcation and oscillation indices satisfy $n' = n$ and $m' = 1$, respectively. Studying these reconnections revealed that the correct way to number the eigenvalues $\omega_{N',n'}$ was to split the double eigenvalues with $n' < N'$ apart as we did in (12) by simultaneously diagonalizing the shift operator and ordering the $\omega_{N',n'}$ via the stride offset of the corresponding eigenvectors (rather than monotonically). Using this ordering, the nontrivial solutions connect up with the N'-hump traveling wave along the $z_{N',n'}$ direction (without involving $z_{N',N'-n'}$). These results are summarized as

$$\begin{aligned} b:&\quad (1,0,2,1) \quad\longleftrightarrow\quad (3,-1,2,1),\\ c:&\quad (1,0,3,1) \quad\longleftrightarrow\quad (4,-1,3,1),\\ d:&\quad (1,0,4,1) \quad\longleftrightarrow\quad (5,-1,4,1). \end{aligned} \tag{39}$$

The labels a, b, c, d in (38) and (39) correspond to the paths labeled $7d$, $8d$, $5c$, a, etc. in the bifurcation diagram. When an integer p precedes a label, it means that the period T that is plotted is p times larger than the fundamental period of the solution represented. Thus, curve $7d$ is the image of curve d (not shown) under the linear transformation $(T, a_2) \mapsto (7T, a_2)$. In our labeling scheme, we just need to multiply ν, m, ν', m' by p to obtain the new path, for example,

$$7d: \quad (1,0,4,7) \quad\longleftrightarrow\quad (5,-7,4,7). \tag{40}$$

In this diagram, we plot $a_2(0)$ versus T with the spatial and temporal phases chosen so the solution is even at $t = 0$. For example, on path d, as we decrease $\rho = a_2(0)$ from 0.371087 to 0, the solution transitions from the one-hump stationary solution to the five-hump left-traveling wave as shown in Figure 2.

It is interesting that the paths labeled a and $3b$ in Figure 1 meet the one-hump stationary solutions in a pitchfork, while the other paths (such as $5c$ and $8d$) meet at an oblique angle from one side only. This is because the second Fourier mode of the eigenvector $z_{1,n}(x)$ in the linearization about the stationary solution is zero in these latter cases, so the change in $a_2(0)$ from that of the stationary solution (namely, 0.371087) is a higher-order effect, (as is the change in T). This explains the oblique angle. We now explain why these bifurcations occur from one side only. When we go beyond the linearization as we have here, we find that $c_2(t) = a_2(t) + i b_2(t)$ has a nearly circular (epitrochoidal) orbit in case a, a circular orbit in case b, and remains constant in time in cases c and d (see Section 4). If one branch of the pitchfork

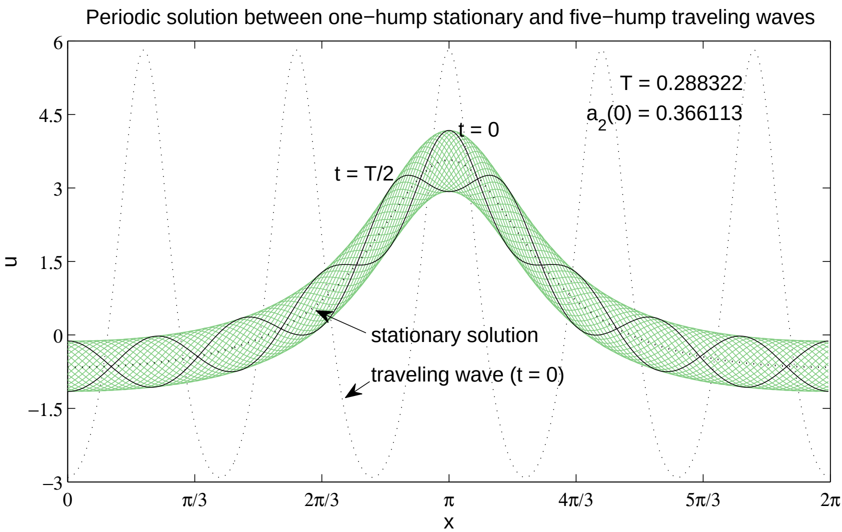

Figure 2. Periodic solution on path d connecting the one-hump stationary solution to the five-hump left-traveling wave ($\alpha_0 = 0.544375$). The second Fourier mode of $z_{1,4}(x)$ is zero, which explains why $a_2(0) = 0.366113$ for this solution is only 1.35% of the way between the stationary solution $a_2(0) = 0.371087$ and the five-hump traveling wave $a_2(0) = 0$.

corresponds to $a_2(0)$, the other is $a_2(T/2)$ since the function $u(\cdot, T/2)$ also has even symmetry. But in cases c and d, $a_2(0)$ is equal to $a_2(T/2)$ even though the functions $u(\cdot, 0)$ and $u(\cdot, T/2)$ are different. These cases also become pitchforks when a different Fourier coefficient $a_K(0)$ is used as the bifurcation parameter.

Next we compute the first several bifurcations from the two-hump traveling waves with mean $\alpha_0 = 0.544375$ and speed index $\nu = -1$. We set $N = 2$, $\nu = -1$, $n \in \{1, 2, 3, 4\}$ and choose the first several legal m values, i.e., values of m that satisfy the bifurcation rules of Table 1 on page 210. For example, the curves labeled i, j, k and l in Figure 1 correspond to the bifurcations $(2, -1, 4, m)$ with $m = 11, 13, 15, 17$; smaller values (and even values) of m are not allowed. In addition to the path a in (38) above, we obtain the paths

$$\begin{aligned}
&e : (2,-1,2,3) \leftrightarrow (3,-3,1,3), && i : (2,-1,4,11) \leftrightarrow (5,-8,3,11),\\
&f : (2,-1,3,6) \leftrightarrow (4,-5,2,6), && j : (2,-1,4,13) \leftrightarrow (5,-9,3,13),\\
&g : (2,-1,3,8) \leftrightarrow (4,-6,2,8), && k : (2,-1,4,15) \leftrightarrow (5,-10,3,15),\\
&h : (2,-1,3,10) \leftrightarrow (4,-7,2,10), && l : (2,-1,4,17) \leftrightarrow (5,-11,3,17).
\end{aligned} \tag{41}$$

The paths f, g and h meet the curve representing the two-hump traveling waves in a pitchfork bifurcation while the others meet obliquely from one side. This, again, is an anomaly of having chosen the second Fourier mode for the bifurcation parameter. The dotted line near the path e is the curve obtained when e is reflected across the T-axis. Solutions on this dotted line correspond to solutions on path e shifted by $\pi/2$ in space, which changes the sign of $\rho = a_2(0)$ but also breaks the even symmetry of the solution at $t = 0$. The paths labeled i, j, k and l are exactly symmetric when reflected about the T-axis because $c_2(t)$ has a circular orbit centered at zero in these cases. It is interesting that so many of the paths in this bifurcation diagram terminate when $T = \pi$ (or a simple rational multiple of π). This is due to the fact that T in (A.1) in Appendix A is independent of α when $n < N$.

The solutions $u(x,t)$ corresponding to points along the paths b, c and d are qualitatively similar to each other. As shown in Figure 2, these solutions look like N'-hump waves traveling over a stationary one-hump carrier signal. At one end of the path the high frequency wave may be viewed as a perturbation of the one-hump stationary solution, while at the other end of the path it is more appropriate to regard the stationary solution as the perturbation, causing the traveling wave to bulge upward as it passes near $x = \pi$ and downward near $x = 0$ and $x = 2\pi$. In all these cases, the solution repeats itself when one of the high frequency waves has moved left one slot to assume the shape of its left neighbor at $t = 0$.

By contrast, the solutions that bifurcate from the two-hump traveling waves, that is, those on the paths listed in (41), have the property that when a wave has moved left one slot to the location that its neighbor occupied at $t = 0$, it has acquired a different shape and must keep progressing a number of slots before it finally lines up with one of the initial waves. This is illustrated in Figure 3 for the solution labeled P in Figure 1 on the path

$$e: \quad (2, -1, 2, 3) \quad \longleftrightarrow \quad (3, -3, 1, 3). \tag{42}$$

This solution is qualitatively similar to the linearized solution $(3, -3, 1, 3)$. There are $N' = 3$ humps oscillating with the same amplitude but with different phases as they travel left. They do not line up with the initial condition again until they have traveled three slots ($\nu' = -3$) and progressed through one cycle ($m'/N' = 3/3$), which leads to a braided effect when the time history of the solution is plotted on one graph. All the solutions on path e are *irreducible* in the sense that there is no smaller time T in which they are periodic (unlike the cases labeled $3b$, $5c$, $7d$, etc. in Figure 1, which are reducible to b, c and d, respectively). Note that although $\nu' = -3$ and $m' = 3$ are both divisible by 3, we cannot reduce $(3, -3, 1, 3)$ to $(3, -1, 1, 1)$ as the latter indices violate the bifurcation rules of Table 1 (page 210). We also mention that at the beginning of the path, near $(2, -1, 2, 3)$, the braiding effect is not present; instead, the solution can be described as two humps bouncing out of phase as they travel left. In one period, they each travel left one slot ($\nu = -1$)

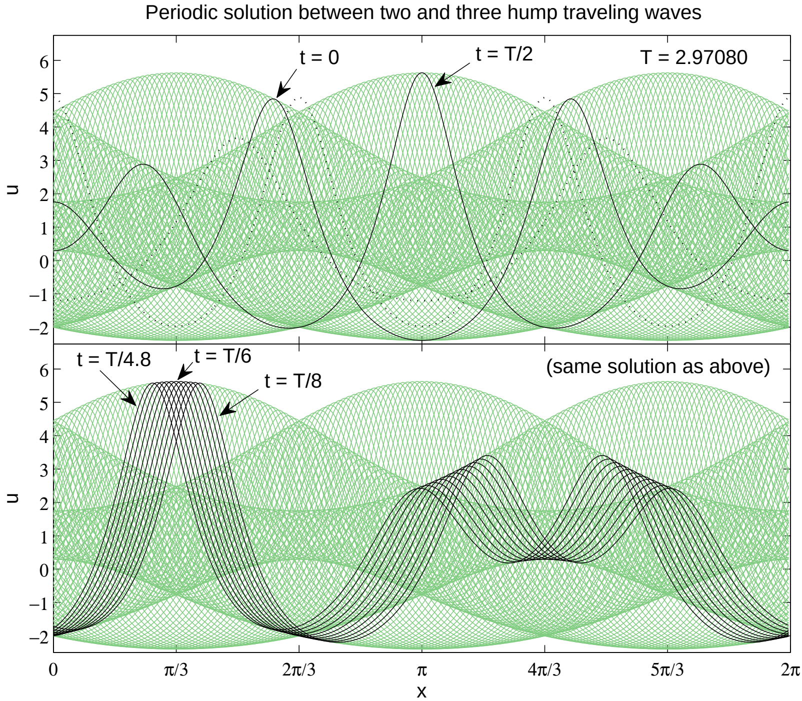

Figure 3. Time-periodic solution (labeled P in Figure 1) on path e connecting two- and three-hump traveling waves. The amplitude of each hump oscillates as it travels left. The dotted curves in the top panel represent the traveling waves at each end of the path at $t = 0$.

and bounce 1.5 times ($m/N = 3/2$) to assume the shape of the other hump at $t = 0$. The transition from this behavior to the braided behavior occurs at the point on path e that a third hump becomes recognizable in the wave profile. The solutions on the paths f, g, h, i, j, k and l are similar to those on path e, but the braiding patterns are more complicated near the right end-points of these paths.

All the traveling waves we have described until now move left. To see what happens to a right-moving wave, we computed the first bifurcation from the simplest such case and obtained the path

$$(1, 1, 1, 2) \quad \longleftrightarrow \quad (2, 0, 1, 2). \tag{43}$$

Thus, the one-hump right-traveling wave is connected to the two-hump stationary solution. Solutions near the left end of this path consist of a large-amplitude, right-moving soliton traveling over a small-amplitude, left-moving soliton. As we progress along the path, the amplitude of the left-moving soliton increases until the solitons cease to fully merge at $t = T/4$ and $t = 3T/4$. Instead, a dimple forms in the

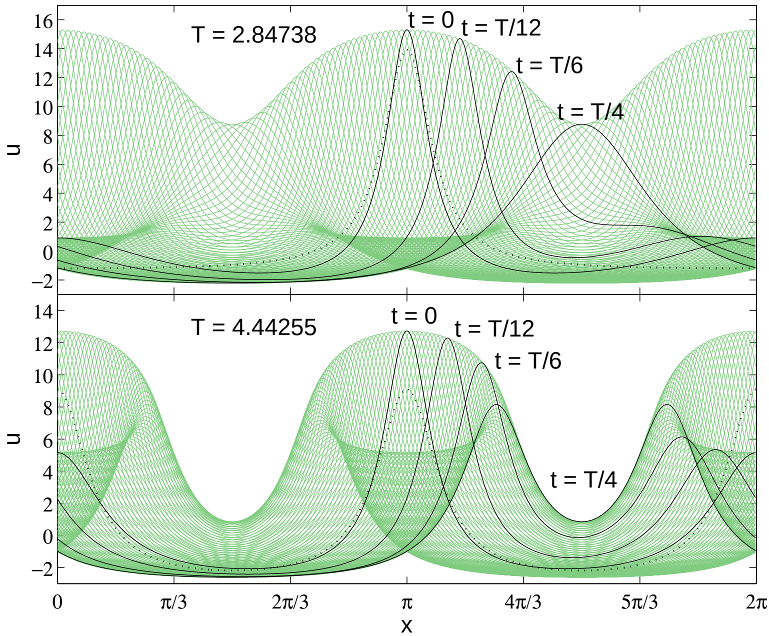

Figure 4. Periodic solutions with mean $\alpha_0 = 0.544375$ between the one-hump right-traveling wave (dotted curve, top panel) and the two-hump stationary solution (dotted curve, bottom panel). Top: a large, right-traveling soliton temporarily merges with a small, left traveling soliton at $t = \frac{1}{4}T$ and $t = \frac{3}{4}T$. Bottom: two solitons traveling in opposite directions bounce off each other at $\frac{1}{4}T$ and $\frac{3}{4}T$ and change direction.

wave profile at these times and the solitons begin to bounce off each other, trading amplitude so the right-moving wave is larger than the left-moving wave. This type of behavior has also been observed by Leveque [22] for the KdV equation for solitons of nearly equal amplitude. Both types of behavior (merging and bouncing off one another) are illustrated in Figure 4. As we proceed further along this path, the solitons settle into a synchronized dancing motion without changing their shape or deviating far from their initial positions. Eventually the "dancing amplitude" becomes small and the nontrivial solution turns into a stationary two-hump solution.

In order to guess a general formula for the relationship between two traveling waves that are connected by a path of nontrivial solutions, we generated two additional paths, namely,

$$\begin{aligned} (2, 0, 2, 2) \quad &\longleftrightarrow \quad (3, -1, 1, 2), \\ (3, 0, 3, 3) \quad &\longleftrightarrow \quad (4, -1, 1, 3). \end{aligned} \tag{44}$$

After studying all the paths listed in (38)–(44), we propose the following conjecture, which we prove as part of Theorem 3 in Section 4:

Conjecture 2. The four-parameter sheet of nontrivial solutions with bifurcation parameters (N, ν, n, m) coincides with the sheet with parameters (N', ν', n', m') if and only if

$$\text{if } n < N: \quad N' = N - n, \quad \nu' = \frac{(N-n)\nu + m}{N}, \quad n' = N - 1, \qquad m' = m, \tag{45}$$

$$\text{if } n \geq N: \quad N' = n + 1, \quad \nu' = \frac{(n+1)\nu - m}{N}, \quad n' = n + 1 - N, \quad m' = m. \tag{46}$$

By symmetry, we may interchange the primed and unprimed indices in either formula; thus, $N' > N \Leftrightarrow n < N \Leftrightarrow n' \geq N'$. In most of our numerical calculations, N' turned out to be larger than N. In the exact formulas of Section 4, we find it more convenient to adopt the convention that $N' < N$ since, in that case, all the solutions on the path connecting these traveling waves turn out to be N-particle solutions as described in Section 2.1.

Equations (45) and (46) are consistent with the bifurcation rules of Appendix A in that

$$n < N, \;\; m \in n\nu + N\mathbb{Z} \quad \Rightarrow \quad \nu' \in \mathbb{Z}, \;\; m' \in (n'+1)\nu' + N'\mathbb{Z}, \tag{47}$$

$$n \geq N, \;\; m \in (n+1)\nu + N\mathbb{Z} \quad \Rightarrow \quad \nu' \in \mathbb{Z}, \;\; m' \in n'\nu' + N'\mathbb{Z}. \tag{48}$$

However, if the mean is held constant, they do not necessarily respect the requirements on α_0 listed in Table 1 (page 210). For example, if $\alpha_0 \leq 3$, then (2, 1, 1, 1) is a valid bifurcation, but the reconnection (1, 1, 1, 1) predicted by (45) is legal only if $\alpha_0 = 3$. Interestingly, when we use our numerical method to follow the path of nontrivial solutions that bifurcates from (2, 1, 1, 1) with the mean $\alpha_0 = 1.2$ held constant, it does not connect up with another traveling wave. Instead, as illustrated in Figure 5, as we vary the bifurcation parameter, the two humps (of the solutions labeled A,B,C) grow in amplitude and merge together until they become a single soliton traveling very rapidly on top of a small amplitude stationary hump. As the bifurcation parameter $\rho = a_1(0)$ approaches a critical value, the period T approaches zero and the solution blows up in $L^2(0, 2\pi)$ with the Fourier coefficients of any time-slice decaying more and more slowly.

As another example, the bifurcation (3, 1, 1, 1) is valid when $\alpha_0 \leq 5$ but the reconnection (2, 1, 2, 1) is only valid if $\alpha_0 = 5$. If we hold $\alpha_0 < 5$ constant, the solution blows up as we vary $\rho = a_2(0)$ from 0 to a critical value. However, *if we simultaneously vary the mean* so that it approaches 5, we do indeed reach a traveling wave with bifurcation indices (2, 1, 2, 1). To check this numerically, we started at (3, 1, 1, 1) with $\alpha_0 = 4.8$ (which has $\alpha = \frac{14}{15}$, $|\beta| = 1/\sqrt{31}$) and computed 40 solutions varying ρ from 0 to 0.1 and setting $\alpha_0 = 4.8 + 2\rho$. The

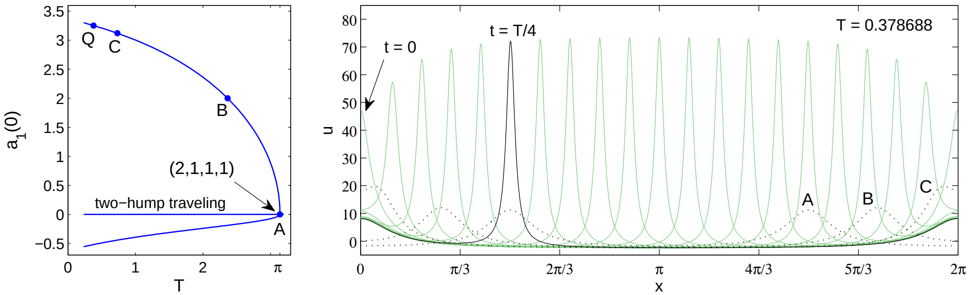

Figure 5. Left: path of nontrivial solutions with mean $\alpha_0 = 1.2$ that bifurcates with indices (2, 1, 1, 1) from the two-hump traveling wave. These solutions do not reconnect with another traveling wave, but instead blow up as $T \to 0$. The solution Q is shown at right, where a large, right-moving soliton travels rapidly over a small, stationary hump. The dotted curves are initial conditions for the points labeled A, B, C at left.

bifurcation at the other end turned out to be (2, 1, 2, 1) with $\alpha_0 = 5$, $\beta = \frac{1}{4}\rho = 0.025$, $\alpha = (1-3\beta^2)/(1-\beta^2)$, $T = \pi/(5-2\alpha)$, as predicted by Conjecture 2. The solutions on this path have the interesting property that the envelope of the solution pinches off into a football shape at one point in the transition from the three-hump traveling wave to the two-hump traveling wave. Using a bracketing technique, we were able to find a solution such that the value of $u(0, t)$ remained constant in time to 8 digits of accuracy. The result is shown in Figure 6.

In summary, it appears that the family of bifurcations with indices (N, ν, n, m) is always connected to the family with indices (N', ν', n', m') given by (45) and (46) by a sheet of nontrivial solutions, but we often have to vary both the mean and

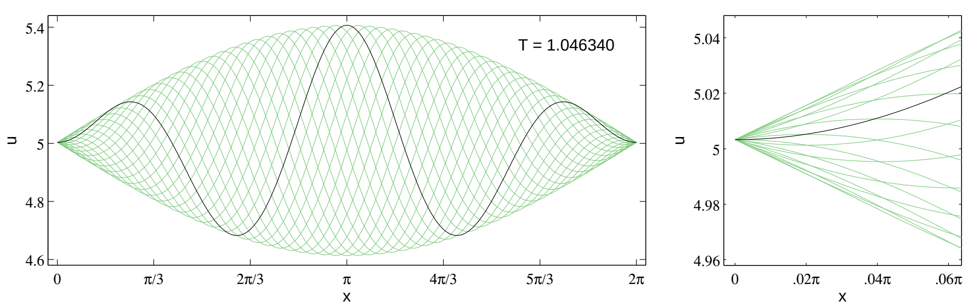

Figure 6. Left: one of the solutions on the path from $\{(3, 1, 1, 1),$ $\beta = -\sqrt{1/31}\}$ to $\{(2, 1, 2, 1),\ \beta = \frac{1}{40}\}$ consists of a traveling wave inside a football-shaped envelope. The exact solution appears to be of the form $u(x, t) = A + B\left(\sin \frac{x}{2}\right) \sin\left(\frac{5}{2}x - \frac{2\pi}{T}t\right)$.

a Fourier coefficient of the initial condition to achieve a reconnection. Thus, the manifold of nontrivial solutions is genuinely two-dimensional (or four dimensional if phase shifts are included). Some of its important properties cannot be seen if we hold the mean α_0 constant.

4. Exact solutions

In this section we use data fitting techniques to determine the analytic form of the numerical solutions of Section 3. We then state a theorem that confirms our numerical predictions and explains why some paths of solutions reconnect with traveling waves when the mean is held fixed while others lead to blow-up. The theorem is proved in Appendix B.

4.1. *Fourier coefficients and lattice sums.* One striking feature of the time-periodic solutions we have found numerically is that the trajectories of the Fourier modes $c_k(t)$ are often circular or nearly circular. Other Fourier modes have more complicated trajectories resembling cartioids, flowers and many other familiar "spirograph" patterns (see Figure 7). This led us to experiment with data fitting to try to guess the analytic form of these solutions. The first thing we noticed was that the trajectories of the spatial Fourier coefficients are band-limited in time, with the width of the band growing linearly with the wave number:

$$u(x,t)=\sum_{k=-\infty}^{\infty} c_k(t)e^{ikx}, \quad c_k(t)=\sum_{j=-\infty}^{\infty} c_{kj}e^{-ij\frac{2\pi}{T}t}, \quad c_{kj}=0 \text{ if } |j|>r|k|. \tag{49}$$

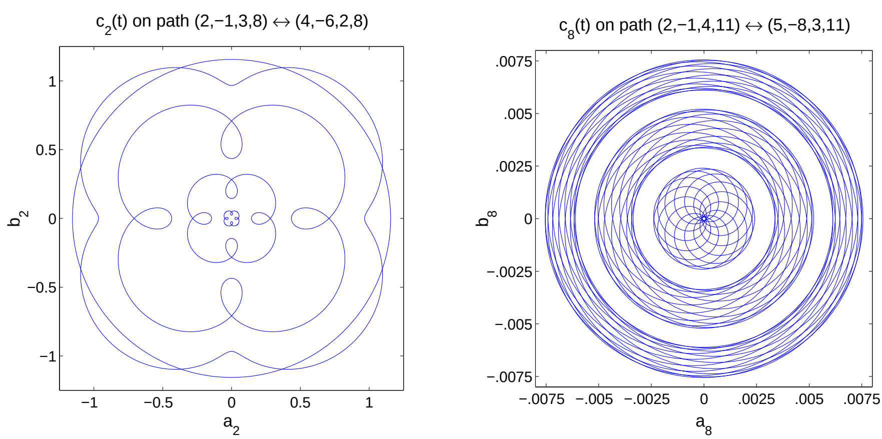

Figure 7. Left: trajectories $c_2(t)$ for five solutions on path g in (41). The evolution of $c_2(t)$ on paths f and h in (41) are similar, but with three- and five-fold symmetry rather than four. Right: trajectories $c_8(t)$ for three solutions on path i in (41).

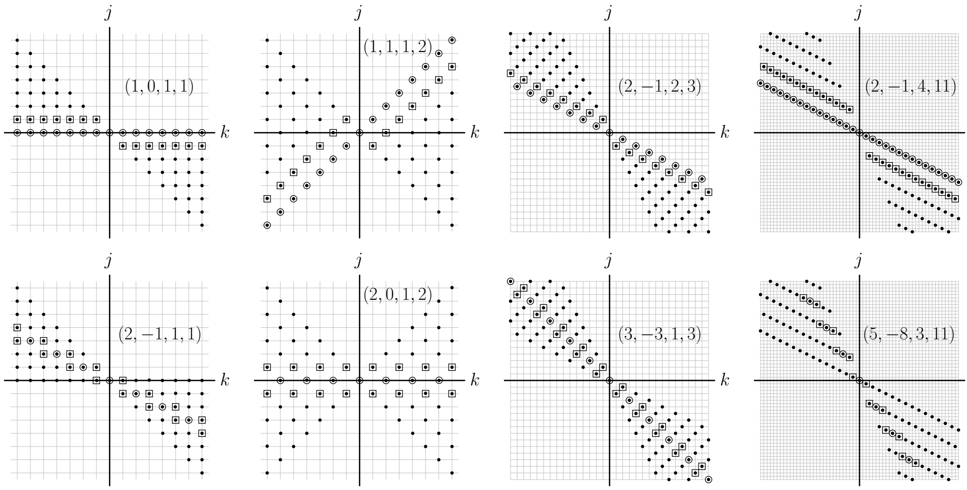

Figure 8. Each pair (aligned vertically) corresponds to a path of nontrivial solutions connecting two traveling waves. Solid dots represent the nonzero entries c_{kj} in (49) of the exact solutions along this path; open circles represent a traveling wave; and open squares represent the nonzero entries d_{kj} in the linearization about the traveling wave.

Here r is a fixed positive integer (depending on which path of nontrivial solutions u belongs to) and the c_{kj} are real numbers when a suitable choice of spatial and temporal phase is made. Since u is real, these coefficients satisfy $c_{-k,-j} = c_{kj}$.

Each path of nontrivial time-periodic solutions has a lattice pattern of nonzero Fourier coefficients c_{kj} associated with it. In Figure 8, we show the lattice of integers (k, j) such that $c_{kj} \neq 0$ for solutions on the paths

$$\begin{aligned} &(1,0,1,1) \longleftrightarrow (2,-1,1,1), \qquad (2,-1,2,3) \longleftrightarrow (3,-3,1,3), \\ &(1,1,1,2) \longleftrightarrow (2,0,1,2), \qquad (2,-1,4,11) \longleftrightarrow (5,-8,3,11). \end{aligned} \tag{50}$$

All solutions on a given path have the same lattice pattern (of solid dots), but different paths have different patterns. One may show that if $u(x,t)$ is of the form (49) and

$$\frac{k}{2}\sum_{l,p} c_{lp}c_{k-l,j-p} = \Big(k|k| + \frac{2\pi}{T}j\Big)c_{kj}, \quad (k > 0,\ j \in \mathbb{Z}), \tag{51}$$

then $u(x,t)$ satisfies the Benjamin–Ono equation, $uu_x = Hu_{xx} - u_t$. The traveling waves at each end of the path have fewer nonzero entries, namely,

$$\tilde{c}_{kj} = \left\{ \begin{array}{ll} N\alpha + \dfrac{2\pi\nu}{NT}, & k = j = 0, \\ 2N\beta^{|k|/N}, & k \in N\mathbb{Z}\setminus\{0\},\ j = \dfrac{\nu k}{N} \\ 0, & \text{otherwise.} \end{array} \right\} \quad \Big(\alpha = \frac{1-3\beta^2}{1-\beta^2}\Big). \tag{52}$$

Here a tilde is used to indicate a solution about which we linearize. Substitution of $c_{kj} = \tilde{c}_{kj} + \varepsilon d_{kj}$ into (51) and matching terms of order ε leads to an eigenvalue problem with solution

$$d_{kj} = \begin{cases} \hat{z}_{N,n}(k), & k \in k_{N,n} + N\mathbb{Z}, \quad j = (k\nu - m)/N, \\ \hat{z}_{N,n}(-k), & k \in -k_{N,n} + N\mathbb{Z}, \quad j = (k\nu + m)/N, \\ 0, & \text{otherwise,} \end{cases} \tag{53}$$

with $\hat{z}_{N,n}(k)$ as in (15). The nonzero coefficients d_{kj} in this linearization are represented by open squares in Figure 8. Recall from (15) that if $n \geq N$ and $k \leq n - N$ then $\hat{z}_{N,n}(k) = 0$, but if $n < N$, the nonzero entries of $\hat{z}_{N,n}(k)$ continue in both directions (with k approaching $+\infty$ or $-\infty$). This is why the rows of open squares terminate in the graphs in the top row of Figure 8 rather than continuing past the origin as in the graphs in the bottom row.

4.2. ***Elementary symmetric functions.*** It is interesting that the lattice patterns that arise for the exact solutions (beyond the linearization) contain only positive integer combinations of the lattice points of the linearization and of the traveling wave (treating the left and right half-planes separately). Somehow the double convolution in (51) leads to exact cancellation at all other lattice sites! This suggests that the c_{kj} have a highly regular structure that generalizes the simple power law decay rate of the Fourier coefficients $\hat{u}_{\text{stat}}(k; N, \beta)$ of the N-hump stationary solution.

The first step to understand this is to grasp that there is a close connection between the trajectories of the Fourier coefficients and the trajectories of the elementary symmetric functions of the particles $\beta_1, \ldots, \beta_N$ in (2). Specifically, because the Fourier coefficients of $\phi(x; \beta)$ in (4) are of the form $2\beta^k$ for $k \geq 1$, we have

$$\beta_1^k(t) + \cdots + \beta_N^k(t) = (1/2)c_k(t), \quad \Big(k \geq 1,\ c_k(t) = \frac{1}{2\pi}\int_0^{2\pi} u(x,t)e^{-ikx}\,dx\Big). \tag{54}$$

Next we define the elementary symmetric functions σ_j via

$$\sigma_0 = 1, \quad \sigma_j = \sum_{l_1 < \cdots < l_j} \beta_{l_1} \cdots \beta_{l_j}, \quad (j = 1, \ldots, N), \tag{55}$$

so that

$$P(z) := \prod_{l=1}^{N} (z - \beta_l) = \sum_{j=0}^{N} (-1)^j \sigma_j z^{N-j}. \tag{56}$$

It is well known [38] that the companion matrix Σ of P has the Jordan canonical form

$$\Sigma = \begin{pmatrix} 0 & 1 & & \\ & \ddots & \ddots & \\ 0 & \cdots & 0 & 1 \\ \pm\sigma_N & \cdots & -\sigma_2 & \sigma_1 \end{pmatrix}, \quad V^{-1}\Sigma V = \begin{pmatrix} J_1 & & \\ & \ddots & \\ & & J_m \end{pmatrix}, \quad J_r = \begin{pmatrix} \beta_{l(r)} & 1 & 0 \\ 0 & \ddots & 1 \\ 0 & 0 & \beta_{l(r)} \end{pmatrix},$$

where $l : \{1, \dots, m\} \to \{1, \dots, N\}$ is an enumeration of the *distinct* roots of $P(z) = 0$ and the size of the Jordan block J_r is equal to the multiplicity of $\beta_{l(r)}$. As a result, the trace of powers of Σ will give the power sums of the β_l, and hence the Fourier coefficients:

$$c_k = 2\,\mathrm{tr}(\Sigma^k), \quad (k \ge 1). \tag{57}$$

Thus, if the elementary symmetric functions are finite sums of circular orbits, then the Fourier coefficients will be as well, and we expect higher Fourier modes to involve more terms, in accordance with our findings above.

Before presenting our main result, we note that once the mapping (45) from (N, ν, n, m) to (N', ν', n', m') is known, we can choose N, ν, N' and ν' independently, subject to the conditions

$$N' < N, \quad \nu' > \frac{N'}{N}\nu. \tag{58}$$

The first condition is merely a labeling convention while the second is an actual restriction on which traveling waves are connected together by a path of nontrivial solutions. The formulas of Conjecture 2 then imply that

$$m = m' = N\nu' - N'\nu > 0, \quad n = N - N', \quad n' = N - 1. \tag{59}$$

After extensive experimentation with data fitting on the numerical simulations described in Section 3, we arrived at the form (61) below for the polynomial P. We then substituted the ansatz (60) into (1) to obtain algebraic relationships between A, B, C, α_0, ω, N, N', ν and ν', namely, (B.9)–(B.11) in Appendix B. We solved these using Mathematica to obtain formulas for A, B and ω in terms of C, α_0, N, N', ν and ν'. We had to break the analysis into three cases depending on whether ν is less than, equal to, or greater than ν'. By comparing our exact solutions with previously known representations of multiperiodic solutions [26], we found that all three cases could be unified by replacing C and α_0 by two new parameters, ρ and ρ', related to C and α_0 by (62) below. We give a direct proof of the following theorem in Appendix B.

Theorem 3. *Let N, N', ν and ν' be integers with $N > N' > 0$ and $N\nu' - N'\nu > 0$. There is a four-parameter family of time-periodic solutions connecting the traveling* *wave bifurcations* $(N', \nu', N-1, m)$ *and* $(N, \nu, N-N', m)$, *where* $m = N\nu' - N'\nu$. *These solutions are of the form*

$$u(x,t) = \alpha_0 + \sum_{l=1}^{N} \phi(x; \beta_l(t)), \qquad \hat{\phi}(k;\beta) = \begin{cases} 2\bar{\beta}^{|k|}, & k < 0, \\ 0, & k = 0, \\ 2\beta^k, & k > 0, \end{cases} \tag{60}$$

where $\beta_1(t), \dots, \beta_N(t)$ *are the roots of the polynomial*

$$P(z) = z^N + Ae^{-i\nu'\omega t} z^{N-N'} + Be^{-i(\nu-\nu')\omega t} z^{N'} + Ce^{-i\nu\omega t}, \tag{61}$$

with

$$\begin{aligned}
A &= e^{i\nu'\omega t_0} e^{-iN'x_0} \sqrt{\frac{N-N'+\rho+\rho'}{N+\rho+\rho'}} \sqrt{\frac{(N+\rho')\rho'}{N'(N-N')+(N+\rho')\rho'}}, \\
B &= e^{i(\nu-\nu')\omega t_0} e^{-i(N-N')x_0} \sqrt{\frac{(N+\rho')\rho'}{N'(N-N')+(N+\rho')\rho'}} \sqrt{\frac{\rho}{N-N'+\rho}}, \\
C &= e^{i\nu\omega t_0} e^{-iNx_0} \sqrt{\frac{\rho}{N-N'+\rho}} \sqrt{\frac{N-N'+\rho+\rho'}{N+\rho+\rho'}}, \\
\alpha_0 &= \frac{N^2\nu' - (N')^2\nu}{m} - 2\rho - \frac{2N'(\nu'-\nu)}{m}\rho', \\
\omega &= \frac{2\pi}{T} = \frac{N'(N-N')(N+2\rho')}{m}.
\end{aligned} \tag{62}$$

The four parameters are $\rho \ge 0$, $\rho' \ge 0$, $x_0 \in \mathbb{R}$ and $t_0 \in \mathbb{R}$. The N- and N'-hump traveling waves occur when $\rho' = 0$ and $\rho = 0$, respectively. When both are zero, we obtain the constant solution $u(x,t) \equiv (N^2\nu' - (N')^2\nu)/m$.

Remark 4. The parameters x_0 and t_0 are spatial and temporal phase shifts. A straightforward calculation shows that if u has parameters ρ, ρ', x_0 and t_0 in Theorem 3 while $\tilde{u}$ has parameters ρ, ρ', 0 and 0, then $u(x,t) = \tilde{u}(x-x_0, t-t_0)$.

There are two features of this theorem that are new. First, it had not previously been observed that the dynamics of the Fourier modes of multiperiodic solutions was so simple. And second, in our representation, it is clear that these solutions reduce to traveling waves in the limit as ρ or ρ' approaches zero. By contrast, other representations become indeterminate in the equivalent limit, and are missing a key degree of freedom (the mean) to allow bifurcation between levels of the hierarchy of multiperiodic solutions.

4.3. ***Three types of reconnection.*** We now wish to explain why following a path of nontrivial solutions with the mean α_0 held fixed sometimes leads to reconnection with a different traveling wave and sometimes leads to blow-up of the initial condition. By Theorem 3, α_0 depends on the parameters ρ and ρ' via

$$\alpha_0 = \alpha_0^* - 2\rho - \frac{2N'(\nu'-\nu)}{m}\rho', \quad \alpha_0^* := \frac{N^2\nu' - (N')^2\nu}{m}. \tag{63}$$

If we hold α_0 fixed, then ρ and ρ' must satisfy

$$2\rho + \frac{2N'(\nu'-\nu)}{m}\rho' = (\alpha_0^* - \alpha_0). \tag{64}$$

This is a line in the ρ-ρ'-plane whose intersection with the first quadrant gives the set of legal parameters for a time-periodic solution to exist. We assume the mean is chosen so that this intersection is nonempty. If the ρ- or ρ'-intercept of this line is positive, the corresponding traveling wave bifurcation exists. There are three cases to consider.

Case 1. ($\nu < \nu'$) Both intercepts will be positive as long as $\alpha_0 < \alpha_0^*$. Thus, a reconnection occurs regardless of which side of the path we start on.

Case 2. ($\nu = \nu'$) The line (64) is vertical in this case, so $\rho = (\alpha_0^* - \alpha_0)/2$ remains constant as we vary ρ' from 0 to ∞. As $\rho' \to \infty$, we see from (62) that $T \to 0$, $A \to 1$, and B and C both approach $\sqrt{\rho/(N-N'+\rho)}$. In this limit, N' of the roots β_l lie on the unit circle at $t=0$, indicating that the norm of the initial condition blows up as $\rho' \to \infty$.

Case 3. ($\nu > \nu'$) The line (64) has positive slope in this case. If $\alpha_0 < \alpha_0^*$, a bifurcation from the N'-hump traveling wave exists. If $\alpha_0 > \alpha_0^*$, a bifurcation from the N-hump traveling wave exists. And if $\alpha_0 = \alpha_0^*$, a bifurcation directly from the constant solution $u = \alpha_0^*$ to a nontrivial time periodic solution exists. In any of these cases, another traveling wave is not reached as we increase ρ and ρ' to ∞. Instead, $T \to 0$ and A, B and C all approach 1. As a result, all the roots β_l approach the unit circle, indicating that the norm of the initial condition blows up as $\rho, \rho' \to \infty$.

Example 5. Consider the three-particle solutions on the path $e : (2,-1,2,3) \leftrightarrow (3,-3,1,3)$ in Figures 1 and 3. Since $-3 = \nu < \nu' = -1$, we do not need to vary the mean in order to reconnect with a traveling wave on the other side of the path. Suppose $\alpha_0 < \alpha_0^* = 1$ is held fixed. Then the parameters ρ and ρ' in Theorem 3 satisfy

$$\rho = \frac{1}{2}\Big(1 - \alpha_0 - \frac{8}{3}\rho'\Big), \quad 0 \le \rho' \le \frac{3(1-\alpha_0)}{8}. \tag{65}$$

The solutions $u(x,t)$ on this path are of the form (60) with particles $\beta_l(t)$ evolving as the roots of the polynomial

$$P(z) = z^3 + Ae^{i\omega t}z + Be^{2i\omega t}z^2 + Ce^{3i\omega t}, \tag{66}$$

where

$$A = \sqrt{\frac{(9-3\alpha_0-2\rho')(3+\rho')\rho'}{(21-3\alpha_0-2\rho')(2+\rho')(1+\rho')}},$$
$$B = \sqrt{\frac{(3-3\alpha_0-8\rho')(3+\rho')\rho'}{(9-3\alpha_0-8\rho')(2+\rho')(1+\rho')}},$$
$$C = \sqrt{\frac{(9-3\alpha_0-2\rho')(3-3\alpha_0-8\rho')}{(21-3\alpha_0-2\rho')(9-3\alpha_0-8\rho')}}, \tag{67}$$
$$\omega = \frac{2\pi}{T} = \frac{2(3+2\rho')}{3}.$$

The transition from the two- to three-hump traveling wave occurs as we decrease the bifurcation parameter ρ' from $3(1-\alpha_0)/8$ to 0. This causes C to increase from 0 to $\sqrt{(1-\alpha_0)/(7-\alpha_0)}$ and A to decrease from $\sqrt{(3-3\alpha_0)/(19-3\alpha_0)}$ to 0. B is zero at both ends of the path.

The trajectories $\beta_1(t)$, $\beta_2(t)$ and $\beta_3(t)$ for $\alpha_0 = 0.544375$ and four choices of ρ' are shown in Figure 9. For this value of the mean, ρ' varies from 0.17086 to 0. Note that the bifurcation from the two-hump traveling wave causes a new particle to nucleate at the origin. As ρ' decreases, the new particle's trajectory grows in amplitude until it joins up with the orbits of the outer particles. There is a critical value of ρ' at which the particles collide and the solution of the ODE (3) ceases to exist for all time; nevertheless, the representation of u in terms of P in (B.1) in Appendix B remains well-behaved and does satisfy (1) for all time. Thus, a change in topology of the orbits does not manifest itself as a singularity in the solution of the

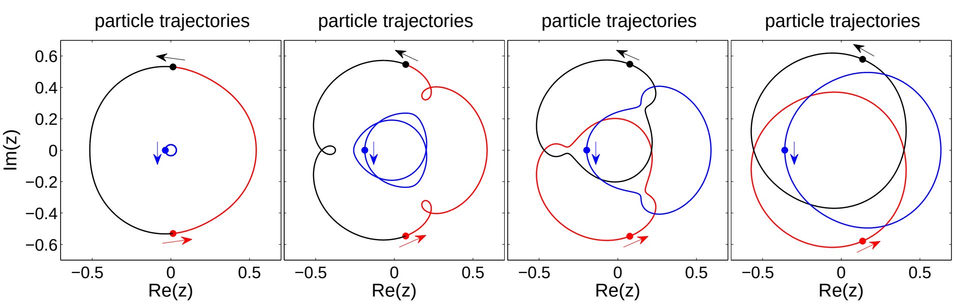

Figure 9. Trajectories $\beta_l(t)$ for four solutions on the path $(2,-1,2,3) \leftrightarrow (3,-3,1,3)$ with mean $\alpha_0 = 0.544375$. The markers give the position of the β_l at $t = 0$. The value of ρ' in (65) is, from left to right: 0.1707, 0.1642, 0.1634 and 0.1369. In Figure 3, $\rho' = 0.0862$.

PDE. As ρ' decreases further, the three orbits become nearly circular and eventually coalesce into a single circular orbit (with $\nu = -3$) at the three-hump traveling wave. The "braided" effect of the solution shown in Figure 3 is recognizable for $\rho' \le 0.15$ or so for this value of the mean.

5. Interior bifurcations

We conclude this work by mentioning that our numerical method for following paths of nontrivial solutions from one traveling wave to another occasionally wanders off course, following an interior bifurcation rather than reaching the traveling wave on the other side of the original path. These interior bifurcations lead to new paths of nontrivial solutions that are more complicated than those on the original path. For example, on the path

$$(1, 1, 1, 2) \longleftrightarrow (2, 0, 1, 2), \tag{68}$$

Theorem 3 tells us that the exact solution is a two-particle solution with elementary symmetric functions of the form

$$\sigma_1(t) = -(Ae^{-i\omega t} + Be^{i\omega t}), \quad \sigma_2(t) = C. \tag{69}$$

We freeze $\alpha_0 < \alpha_0^* = 2$, set $\rho = \frac{1}{2}(2 - \alpha_0 - \rho')$, and determine that

$$\begin{aligned}
A &= e^{-i(x_0 - \omega t_0)} \sqrt{\frac{(4 - \alpha_0 + \rho')(2 + \rho')\rho'}{(6 - \alpha_0 + \rho')(1 + \rho')^2}}, \\
B &= e^{-i(x_0 + \omega t_0)} \sqrt{\frac{(2 - \alpha_0 - \rho')(2 + \rho')\rho'}{(4 - \alpha_0 - \rho')(1 + \rho')^2}}, \\
C &= e^{-i(2x_0)} \sqrt{\frac{(4 - \alpha_0 + \rho')(2 - \alpha_0 - \rho')}{(6 - \alpha_0 + \rho')(4 - \alpha_0 - \rho')}}, \\
\omega &= \frac{2\pi}{T} = 1 + \rho'.
\end{aligned} \tag{70}$$

In Figure 10, we show the bifurcation diagram for the transition from the one-hump right-traveling wave (labeled P) to the two-hump stationary solution (labeled Q). This diagram was computed numerically before we had any idea that exact solutions for this problem exist; therefore, we used the real part of the first Fourier mode at $t = 0$ for the bifurcation parameter rather than ρ'. We can obtain the same curves analytically as follows. The upper curve from P to Q (containing A1–A5) can be plotted parametrically by setting $x_0 = \pi/2$ and $t_0 = \pi/2\omega$ in (70), varying ρ' from $2 - \alpha_0$ to 0, holding $\alpha_0 = 0.544375$ fixed, and plotting $-2(A + B)$ versus

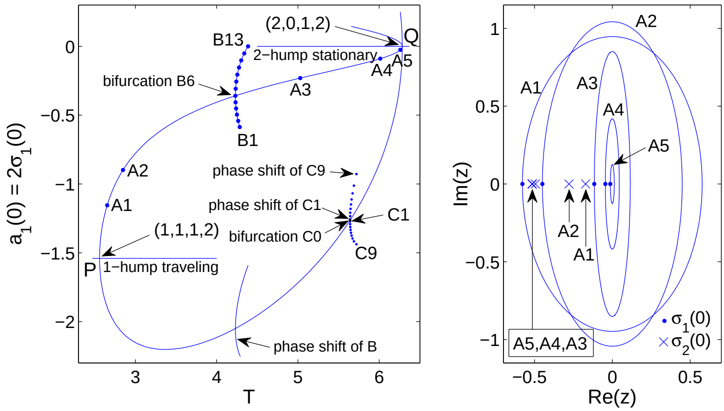

Figure 10. Left: bifurcation diagram showing several interior bifurcations on the path $(1, 1, 1, 2) \to (2, 0, 1, 2)$. Right: trajectories of the elementary symmetric functions $\sigma_1(t)$, which have elliptical, clockwise orbits, and $\sigma_2(t)$, which remain stationary in time, for the solutions labeled A1–A5 in the bifurcation diagram.

$T = 2\pi/(1+\rho')$. The lower curve from P to Q is obtained in the same fashion if we instead set $x_0 = t_0 = 0$.

As illustrated in Figure 10, solutions such as A1–A5 on the upper path have $\sigma_1(t)$ executing elliptical, clockwise orbits that start out circular at the one-hump traveling wave but become more eccentric and collapse to a point as we progress toward the two-hump stationary solution Q. Meanwhile, $\sigma_2(t)$ remains constant in time, nucleating from the origin at the one-hump traveling wave and terminating with $\sigma_2 \equiv -\sqrt{(2-\alpha_0)/(6-\alpha_0)}$ at the two-hump stationary solution. On the lower path, the major axis of the orbit of σ_1 is horizontal rather than vertical and σ_2 moves right rather than left as we move from P to Q.

When computing these paths from P to Q, we encountered two interior bifurcations. In the bifurcation labeled B6 in Figure 10, an additional elementary symmetric function nucleates at the origin and the trajectories of σ_1 and σ_2 become more complicated. Through data fitting, we find that

$$\sigma_1(t) = -(Ae^{-i\omega t} + Be^{i\omega t} + C_1 e^{3i\omega t}), \tag{71}$$

$$\sigma_2(t) = C + C_2 e^{2i\omega t} + C_3 e^{4i\omega t}, \tag{72}$$

$$\sigma_3(t) = -C_4 e^{3i\omega t}, \tag{73}$$

where the new coefficients C_j are all real parameters. We have not attempted to derive algebraic relationships among these parameters to obtain exact solutions. These trajectories are shown in Figure 11 for the solutions labeled B1–B13 in the bifurcation diagram. The additional term in (71) causes the elliptical orbit of $\sigma_1(t)$

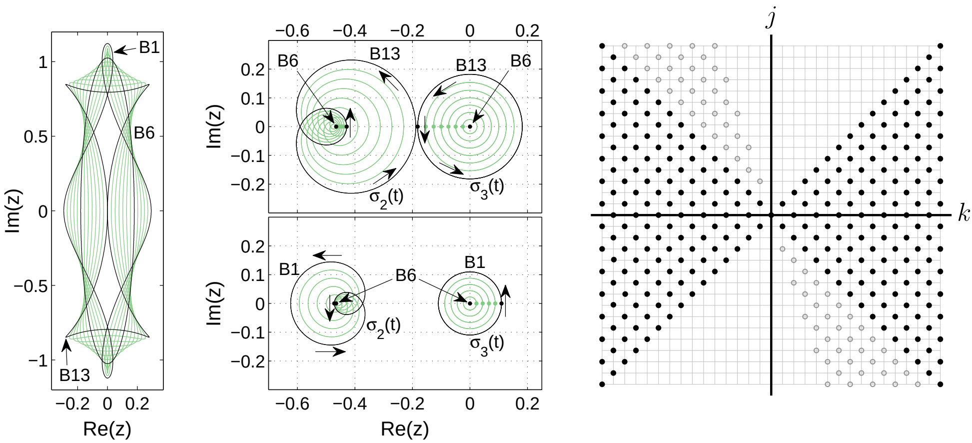

Figure 11. Left: trajectories of $\sigma_1(t)$ for solutions labeled B1–B13 in Figure 10. Center: trajectories of $\sigma_2(t)$ and $\sigma_3(t)$. Since B6 is on the original path from P to Q, $\sigma_2(t)$ is constant and $\sigma_3(t) \equiv 0$ for this solution. Right: the interior bifurcation causes additional lattice coefficients c_{kj} to become nonzero; grey circles represent the new terms.

to deform by bulging out in the vertical and horizontal directions while pulling in along the diagonal directions (or vice versa, depending on which direction we follow the bifurcation). Meanwhile, $\sigma_2(t)$ ceases to be constant and $\sigma_3(t)$ ceases to be zero. To avoid clutter, we plotted the trajectories $\sigma_2(t)$ and $\sigma_3(t)$ for B1–B6 separately from B6–B13, illustrating the effect of following the bifurcation in one direction or the other. The additional terms in (71)–(73) cause the lattice pattern of nonzero entries $c_{kj} = \frac{1}{T}\int_0^T c_k(t)e^{ij\omega t}\,dt$ to become more complicated, where we recall that in this case,

$$c_k(t) = \frac{1}{2\pi}\int_0^{2\pi} u(x,t)e^{-ikx}\,dx = 2\,\mathrm{tr}\left[\begin{pmatrix} 0 & 1 & 0 \\ 0 & 0 & 1 \\ \sigma_3(t) & -\sigma_2(t) & \sigma_1(t)\end{pmatrix}^k\right].$$

The solid dots in Figure 11 represent the nonzero entries of solutions on the original path from P to Q while grey circles show the additional terms that are nonzero after the bifurcation at B6. Although this bifurcation causes some of the unoccupied lattice sites to be filled in, the new lattice pattern is rather similar to the original pattern and maintains its checkerboard structure. Also, this bifurcation leads to symmetric perturbations of the Fourier mode trajectories, and is also present (in a phase shifted form) along the lower path from P to Q.

In the bifurcation labeled C0 in Figure 10, the fill-in pattern of the lattice representation is much more complicated, and in fact the checkerboard structure of the nonzero coefficients c_{kj} is destroyed; see Figure 12. But actually, the elementary symmetric functions behave similarly to the previous case: By fitting our numerical data, we find that

$$\sigma_1(t) = -(Ae^{-i\omega t} + Be^{i\omega t} + C_1 e^{4i\omega t}), \tag{74}$$

$$\sigma_2(t) = C + C_2 e^{3i\omega t} + C_3 e^{5i\omega t}, \tag{75}$$

$$\sigma_3(t) = -C_4 e^{4i\omega t}, \tag{76}$$

so each of the new terms executes one additional loop per cycle of the periodic solution in comparison to the corresponding term in (71)–(73). This extra loop causes a star-shaped perturbation of the σ_1 ellipse instead of the rectangular and diamond shaped perturbations seen previously in Figure 11. As a result, this bifurcation is not present on the upper path from P to Q because the symmetry of the perturbation does not respect the 90 degree rotation of the orbit $\sigma_1(t)$ associated with the $\frac{\pi}{2}$-spatial and $\frac{T}{4}$-temporal phase shifts that relate solutions on the upper and lower paths from P to Q.

To follow the bifurcation at C0 in the other direction, we can use the same numerical values for A, B, C, C_1, C_2, C_3, C_4 in (74)–(76) after changing the signs of the latter four parameters. This causes the trajectories of σ_1 in Figure 12 to be rotated 180° with a corresponding $T/2$ phase-shift in time so that the initial position $\sigma_1(0)$ remains on the left side of the figure. Meanwhile, the trajectory of $\sigma_2(t)$

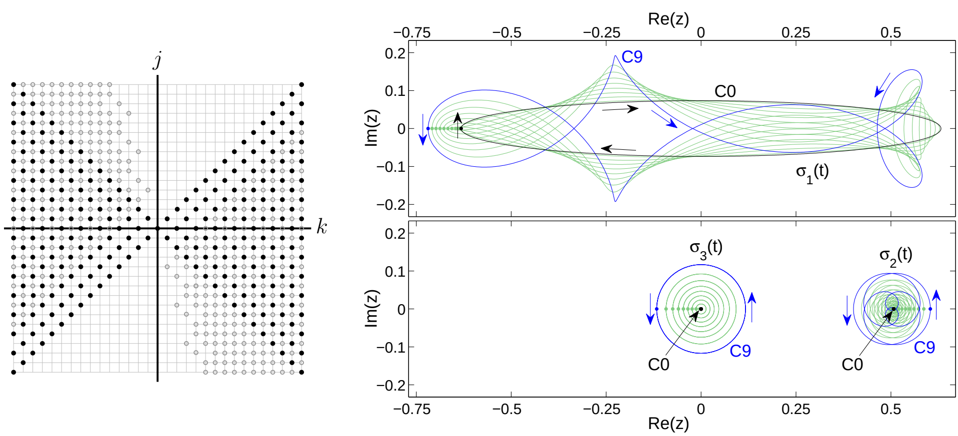

Figure 12. Left: this interior bifurcation causes more lattice coefficients to become nonzero than the interior bifurcation of Figure 11. Right: trajectories of $\sigma_1(t)$, $\sigma_2(t)$, and $\sigma_3(t)$ for the solutions labeled C0-C9 in Figure 10. The long axis of the ellipse C0 is horizontal because we start from the bottom branch connecting P to Q in Figure 10.

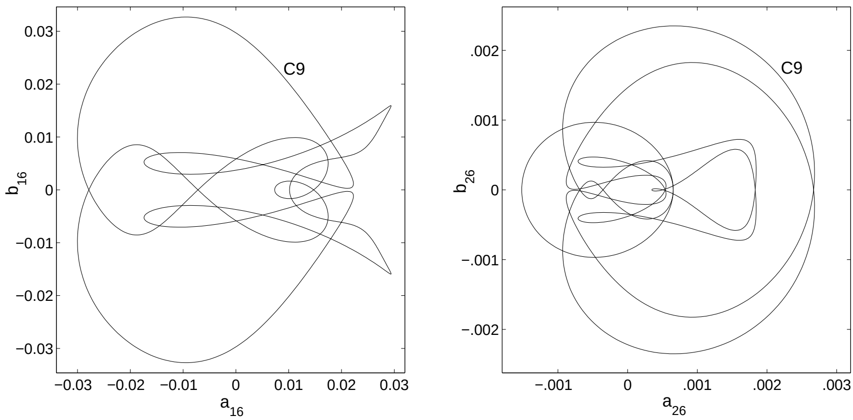

Figure 13. The trajectories of the Fourier modes become very complicated after the interior bifurcation occurs. Here we show the 16th (left) and 26th (right) Fourier modes $c_k(t) = a_k(t) + ib_k(t)$ over one period. It was clearly essential to use a high order (in fact, spectrally accurate) numerical method to resolve these dynamics when computing time-periodic solutions.

experiences a $T/2$ phase-shift in time with no change in the location of the orbit, and $\sigma_3(t)$ starts on the opposite side of its circular trajectory about the origin.

In Figure 13, we show the orbits of the 16th and 26th Fourier modes for the solution labeled C9 in the bifurcation diagram of Figure 10. As the index of the Fourier mode increases, these trajectories become increasingly complicated (involving more nonzero terms c_{kj} in the lattice representation), but also decay exponentially so that the amplitude of the orbit is eventually smaller than can be resolved using floating point arithmetic. We emphasize that these trajectories were resolved to full machine precision by our general purpose numerical method for finding periodic solutions of nonlinear PDE (without any knowledge of the solitonic structure of the solutions). Everything we learned about the form of the exact solutions came about from studying these numerical solutions, which was possible only because our numerical results are correct to 10-15 digits of accuracy.

Appendix A. Bifurcation formulas and rules

In this section we collect formulas relating the period, mean and decay parameter at a bifurcation. We also identify bifurcation rules governing the legal values of α_0 for a given set of bifurcation indices.

In computing the nullspace $\mathcal{N} = \ker DF(U_0, T)$ in Section 2.3, we considered N, ν, β, T (and hence α_0) to be given and searched for compatible indices n and m. The decay parameter $|\beta|$, the mean α_0, and the period T cannot be specified independently; any two of them determines the third. We now derive formulas for the period and mean in terms of (N, ν, n, m) and β. To simplify the formulas, we work with $\alpha = (1-3|\beta|^2)/(1-|\beta|^2)$ instead of β. Note that as we increase $|\beta|$ from 0 to 1, α decreases from 1 to $-\infty$. For the period, we have

$$T = \frac{2\pi m}{N\omega_{N,n}} = \begin{cases} \dfrac{2\pi m}{Nn(N-n)} & n < N, \\ \dfrac{2\pi m}{N(n+1-N)(n+1+N(1-\alpha))} & n \geq N, \end{cases} \tag{A.1}$$

so the period is independent of β when $n < N$, and otherwise decreases to zero as $|\beta|$ varies from 0 to 1. For the mean, α_0, we note that

$$cT = \frac{2\pi\nu}{N}, \quad c = \alpha_0 - N\alpha \quad \Rightarrow \quad \alpha_0 = N\alpha + \frac{2\pi\nu}{NT}. \tag{A.2}$$

Hence, using $(2\pi/NT) = (\omega_{N,n}/m)$, we obtain

$$\alpha_0 = \begin{cases} N + \dfrac{n(N-n)}{m}\nu - (1-\alpha)N, & n < N, \\ N + \dfrac{(n+1-N)(n+1)}{m}\nu - \Big(1 - \dfrac{n+1-N}{m}\nu\Big)N(1-\alpha), & n \geq N. \end{cases} \tag{A.3}$$

Thus, as $|\beta|$ varies from 0 to 1, the mean α_0 decreases to $-\infty$ if $n < N$, and otherwise either decreases to $-\infty$, increases to $+\infty$, or is independent of β, depending on the sign of $[m - (n+1-N)\nu]$.

In practice, we often wish to start with N, ν, n, m and α_0 and determine T and $|\beta|$ from these. However, not all values of α_0 are compatible with a given set of indices. The bifurcation rules are summarized in Table 1.

Solving (A.3) for α yields

$$\alpha = \begin{cases} 1 - \dfrac{(N-\alpha_0)m + n(N-n)\nu}{Nm}, & n < N, \\ 1 - \dfrac{(N-\alpha_0)m + (n+1-N)(n+1)\nu}{[m-(n+1-N)\nu]N}, & n \geq N. \end{cases} \tag{A.4}$$

The corresponding period is given by

$$T = \begin{cases} \dfrac{2\pi m}{Nn(N-n)}, & n < N, \\ \dfrac{2\pi\left(\frac{m}{n+1-N} - \nu\right)}{N(n+1+N-\alpha_0)}, & n \geq N. \end{cases} \tag{A.5}$$

In the indeterminate cases $\{n \geq N,\ m = (n+1-N)\nu,\ \alpha_0 = n+1+N\}$, any $\alpha \leq 1$ is allowed and formula (A.1) should be used to determine T.

If we express n, n', m and m' in terms of N, ν, N', ν', then (A.1) and (A.3) give

$$\begin{aligned} T &= \frac{2\pi(N\nu' - N'\nu)}{N'(N-N')N}, & \alpha_0 &= \alpha_0^* - (1-\alpha)N, \\ T' &= \frac{2\pi(N\nu' - N'\nu)}{N'(N-N')[N+(1-\alpha')N']}, & \alpha_0' &= \alpha_0^* - \frac{\nu' - \nu}{N\nu' - N'\nu}(N')^2(1-\alpha'), \end{aligned} \tag{A.6}$$

where

$$\alpha_0^* = \frac{N^2\nu' - (N')^2\nu}{N\nu' - N'\nu}, \qquad \alpha = \frac{1-3|\beta|^2}{1-|\beta|^2}, \qquad \alpha' = \frac{1-3|\beta'|^2}{1-|\beta'|^2}.$$

We note that the two traveling waves reduce to the same constant function when $\beta \to 0$ and $\beta' \to 0$, which is further evidence that a single sheet of nontrivial solutions connects these two families of traveling waves.

Appendix B. Proof of Theorem 3

As explained in Remark 4, x_0 and t_0 are spatial and temporal phase shifts, so we may set them to zero without loss of generality. We can express the solution directly in terms of the elementary symmetric functions via

$$\begin{aligned} u(x,t) &= \alpha_0 + \sum_{l=1}^{N} \phi(x; \beta_l(t)) = \alpha_0 + \sum_{l=1}^{N} 4\,\mathrm{Re}\Big\{\sum_{k=1}^{\infty} \beta_l(t)^k e^{ikx}\Big\} \\ &= \alpha_0 + \sum_{l=1}^{N} 4\,\mathrm{Re}\Big\{\frac{z}{z-\beta_l(t)} - 1\Big\} = \alpha_0 + 4\,\mathrm{Re}\Big\{\frac{z\partial_z P(z)}{P(z)} - N\Big\},\ (z = e^{-ix}). \end{aligned} \tag{B.1}$$

(1) $N \geq 1,\ \nu \in \mathbb{Z},\ n \geq 1,\ m \geq 1$

(2) if $n < N$ then
- $m \in n\nu + N\mathbb{Z}$
- $\alpha_0 \leq N + n(N-n)\nu/m$

(3) if $n \geq N$ then
- $m \in (n+1)\nu + N\mathbb{Z}$
- if $m > (n+1-N)\nu$ then $\alpha_0 \leq N + (n+1-N)(n+1)\nu/m$
- if $m < (n+1-N)\nu$ then $\alpha_0 \geq N + (n+1-N)(n+1)\nu/m$
- if $m = (n+1-N)\nu$ then $\alpha_0 = n+1+N$

Table 1. Bifurcation rules governing which values of α_0 are compatible with the bifurcation indices (N, ν, n, m).

Next we derive algebraic expressions relating A, B, C, α_0, ω, N, N', ν and ν' by substituting (B.1) into the Benjamin–Ono equation (1). To this end, we include the time dependence of P in the notation and write (B.1) in the form

$$u(x,t)=\alpha_0+2\Big(\frac{i\partial_x g}{g}-N\Big)+2\Big(\frac{-i\partial_x h}{h}-N\Big), \tag{B.2}$$

where

$$g(x,t)=P(e^{-ix},e^{-i\omega t}), \qquad h(x,t)=\overline{g(x,t)}, \tag{B.3}$$

$$P(z,\lambda)=z^N+A\lambda^{\nu'}z^{N-N'}+B\lambda^{\nu-\nu'}z^{N'}+C\lambda^{\nu}. \tag{B.4}$$

Note that P is a polynomial in z and a Laurent polynomial in λ (as ν and ν' may be negative). We may assume $\omega>0$; if not, we can change the sign of ω without changing the solution by replacing (A,B,ν,ν',N') by $(B,A,-\nu,\nu'-\nu,N-N')$. Assuming the roots $\beta_l(t)$ of $z\mapsto P(z,e^{-i\omega t})$ remain inside the unit disk Δ for all t, we have

$$\Big(\frac{i\partial_x g}{g}-N\Big)=\sum_{l=1}^{N}\sum_{k=1}^{\infty}\beta_l(t)^k e^{ikx} \quad\Rightarrow\quad Hu=2\Big(\frac{\partial_x g}{g}+Ni\Big)+2\Big(\frac{\partial_x h}{h}-Ni\Big). \tag{B.5}$$

Using (B.2) and $\partial_t(\partial_x g/g)=\partial_x(\partial_t g/g)$, (a technique we learned by studying the bilinear formalism approach of [32; 26]), the equation $1/2\,(u_t-Hu_{xx}+uu_x)=0$ becomes

$$\partial_x\left[i\Big(\frac{\partial_t g}{g}-\frac{\partial_t h}{h}\Big)-\partial_x\Big(\frac{\partial_x g}{g}+\frac{\partial_x h}{h}\Big)+\frac{1}{4}\Big((\alpha_0-4N)+2i\Big(\frac{\partial_x g}{g}-\frac{\partial_x h}{h}\Big)\Big)^2\right]=0. \tag{B.6}$$

The expression in brackets must be a constant, which we denote by γ. We now write

$$P_{jk}=(z\partial_z)^j(\lambda\partial_\lambda)^k P(z,\lambda)\Big|_{\substack{z=e^{-ix}\\ \lambda=e^{-i\omega t}}} \tag{B.7}$$

so that, for example, $\partial_t g=-i\omega P_{01}$ and $\partial_x h=i\bar{P}_{10}$. Equation (B.6) then becomes

$$\gamma\,P_{00}\bar{P}_{00}+\bar{P}_{00}[P_{20}+\omega P_{01}+(\alpha_0-4N)P_{10}] \\ +P_{00}[\bar{P}_{20}+\omega\bar{P}_{01}+(\alpha_0-4N)\bar{P}_{10}]+2P_{10}\bar{P}_{10}=0, \tag{B.8}$$

where we have absorbed $\frac{1}{4}(\alpha_0-4N)^2$ into γ. This equation may be written

$$e_1[\![z^N\lambda^{-\nu}]\!]+e_2[\![z^{N-2N'}\lambda^{2\nu'-\nu}]\!]+e_3[\![z^{N-N'}\lambda^{\nu'-\nu}]\!]+e_4[\![z^{N'}\lambda^{-\nu'}]\!]+e_5=0,$$

where $[\![a]\!]=a+\bar{a}=2\,\mathrm{Re}\{a\}$,

$$e_1=[\gamma+\nu\omega+N^2+(\alpha_0-4N)N]C, \qquad e_2=[\gamma+\nu\omega+N^2+(\alpha_0-4N)N]AB,$$

and, after setting $\gamma = (3N-\alpha_0)N - \nu\omega$ to achieve $e_1 = e_2 = 0$,

$$e_3 = [(N')^2 - 2NN' + N'\alpha_0 - \nu'\omega]B + [(N')^2 + 2NN' - N'\alpha_0 + \nu'\omega]AC = 0, \quad \text{(B.9)}$$

$$\begin{aligned} e_4 = {} & [3N^2 - 4NN' + (N')^2 - (N-N')\alpha_0 + (\nu - \nu')\omega]BC \\ & -[N^2 - (N')^2 - (N-N')\alpha_0 + (\nu-\nu')\omega]A = 0, \end{aligned} \quad \text{(B.10)}$$

$$\begin{aligned} e_5 = {} & (N\alpha_0 - \nu\omega - N^2) + [(2N'-N)\alpha_0 + (\nu - 2\nu')\omega + 3N^2 - 8NN' + 4(N')^2]B^2 \\ & + [(N-2N')\alpha_0 + 4(N')^2 - N^2 + (2\nu' - \nu)\omega]A^2 + [(3N-\alpha_0)N + \nu\omega]C^2 = 0. \end{aligned} \quad \text{(B.11)}$$

Using a computer algebra system, it is easy to check that (B.9)–(B.11) hold when A, B, C, α_0 and ω are defined as in (62). When $\rho' = 0$, we have $A = B = 0$ and $C = \sqrt{\rho/(N+\rho)}$ so that

$$\beta_l(t) = \sqrt[N]{-C\lambda^\nu} = \sqrt[N]{-C}\, e^{-ict}, \qquad c = \frac{\omega\nu}{N} = \frac{N'(N-N')\nu}{m} = \alpha_0 - N\frac{1-3C^2}{1-C^2},$$

where each β_l is assigned a distinct N-th root of $-C$. By (5), this is an N-hump traveling wave with speed index ν and period $T = 2\pi/\omega$. Similarly, when $\rho = 0$, we have $B = C = 0$ and $A = \sqrt{\rho'/(N'+\rho')}$ so that

$$\beta_l(t) = \left\{ \begin{array}{cc} \sqrt[N']{-A}\, e^{-ict}, & l \le N' \\ 0, & l > N' \end{array} \right\},$$
$$c = \frac{\omega\nu'}{N'} = \frac{(N-N')(N+2\rho')\nu'}{m} = \alpha_0 - N'\frac{1-3A^2}{1-A^2},$$

which is an N'-hump traveling wave with speed index ν' and period $T = 2\pi/\omega$.

Finally, we show that the roots of $P(\,\cdot\,,\lambda)$ are inside the unit disk for any λ on the unit circle, S^1. We will use Rouché's theorem [1]. Let

$$\begin{aligned} f_1(z) &= z^N + A\lambda^{\nu'} z^{N-N'} + B\lambda^{\nu-\nu'} z^{N'} + C\lambda^\nu, \\ f_2(z) &= z^N + A\lambda^{\nu'} z^{N-N'}, \\ f_3(z) &= z^N \qquad\qquad\qquad\quad + B\lambda^{\nu-\nu'} z^{N'}. \end{aligned}$$

From (62), we see that $\{A, B, C\} \subseteq [0, 1)$, $A \ge BC$, $B \ge CA$ and $C \ge AB$. Thus,

$$\begin{aligned} d_2(z) := |f_2(z)|^2 - |f_1(z) - f_2(z)|^2 &= |\lambda^{-\nu'} z^{N'} + A|^2 - |B\lambda^{-\nu'} z^{N'} + C|^2 \\ &= 1 + A^2 - B^2 - C^2 + 2(A - BC)\cos\theta \ge (1-A)^2 - (B-C)^2, \end{aligned} \quad \text{(B.12)}$$

where $\lambda^{-\nu'} z^{N'} = e^{i\theta}$. Similarly,

$$d_3 := |f_3(z)|^2 - |f_1(z) - f_3(z)|^2 \ge (1-B)^2 - (A-C)^2. \quad \text{(B.13)}$$

Note that

$$\begin{array}{llllll} B \le A, & C \le B & \Rightarrow & B - C \le B - AB < 1 - A & \Rightarrow & d_2(z) > 0 \text{ for } z \in S^1, \\ B \le A, & C > B & \Rightarrow & |C - A| < 1 - B & \Rightarrow & d_3(z) > 0 \text{ for } z \in S^1, \\ A \le B, & C \le A & \Rightarrow & A - C \le A - AB < 1 - B & \Rightarrow & d_3(z) > 0 \text{ for } z \in S^1, \\ A \le B, & C > A & \Rightarrow & |C - B| < 1 - A & \Rightarrow & d_2(z) > 0 \text{ for } z \in S^1. \end{array}$$

Thus, in all cases, $f_1(z) = P(z, \lambda)$ has the same number of zeros inside S^1 as $f_2(z)$ or $f_3(z)$, which each have N roots inside S^1. Since $f_1(z)$ is a polynomial of degree N, all the roots are inside S^1.

References

[1] L. V. Ahlfors, *Complex analysis: An introduction to the theory of analytic functions of one complex variable*, 3rd ed., McGraw-Hill, New York, 1978. MR 80c:30001 Zbl 0395.30001

[2] D. M. Ambrose and J. Wilkening, *Time-periodic solutions of the Benjamin-Ono equation*, preprint, 2008. arXiv 0804:3623

[3] ———, *Computation of time-periodic solutions of the vortex sheet with surface tension*, in preparation, 2009.

[4] D. M. Ambrose, *Well-posedness of vortex sheets with surface tension*, SIAM J. Math. Anal. **35** (2003), no. 1, 211–244. MR 2005g:76006 Zbl 1107.76010

[5] C. J. Amick and J. F. Toland, *Uniqueness and related analytic properties for the Benjamin–Ono equation: a nonlinear Neumann problem in the plane*, Acta Math. **167** (1991), no. 1-2, 107–126. MR 92i:35099 Zbl 0755.35108

[6] T. B. Benjamin, *Internal waves of permanent form in fluids of great depth*, J. Fluid Mech. **29** (1967), no. 3, 559–592.

[7] T. L. Bock and M. D. Kruskal, *A two-parameter Miura transformation of the Benjamin–Ono equation*, Phys. Lett. A **74** (1979), no. 3-4, 173–176. MR 82d:35083

[8] M. O. Bristeau, R. Glowinski, and J. Périaux, *Controllability methods for the computation of time-periodic solutions; application to scattering*, J. Comput. Phys. **147** (1998), no. 2, 265–292. MR 99k:65093 Zbl 0926.65054

[9] C. G. Broyden, *The convergence of a class of double-rank minimization algorithms. II. The new algorithm*, J. Inst. Math. Appl. **6** (1970), 222–231. MR 55 #6841 Zbl 0207.17401

[10] M. Cabral and R. Rosa, *Chaos for a damped and forced KdV equation*, Phys. D **192** (2004), no. 3-4, 265–278. MR 2005d:37161 Zbl 1061.35103

[11] R. Camassa and L. Lee, *Complete integrable particle methods and the recurrence of initial states for a nonlinear shallow-water wave equation*, J. Comput. Phys. **227** (2008), no. 15, 7206–7221. MR 2009e:76019 Zbl 05304665

[12] K. M. Case, *Meromorphic solutions of the Benjamin–Ono equation*, Phys. A **96** (1979), no. 1-2, 173–182. MR 80i:35026

[13] ———, *The Benjamin–Ono equation: a remarkable dynamical system*, Ann. Nuclear Energy **7** (1980), no. 4-5, 273–277. MR 82j:76012

[14] G. J. Cooper and A. Sayfy, *Additive Runge–Kutta methods for stiff ordinary differential equations*, Math. Comp. **40** (1983), no. 161, 207–218. MR 84b:65066 Zbl 0525.65053

[15] R. E. Davis and A. Acrivos, *Solitary internal waves in deep water*, J. Fluid Mech. **29** (1967), no. 3, 593–607.

[16] S. Y. Dobrokhotov and I. M. Krichever, *Multi-phase solutions of the Benjamin-Ono equation and their averaging*, Mat. Zametki **49** (1991), 42–58, In Russian; translated in *Math. Notes* **49** (1991), 583–594. MR 92g:35182

[17] E. Doedel, H. B. Keller, and J.-P. Kernévez, *Numerical analysis and control of bifurcation problems, II. Bifurcation in infinite dimensions*, Internat. J. Bifur. Chaos Appl. Sci. Engrg. **1** (1991), no. 4, 745–772. MR 93c:34001b Zbl 0876.65060

[18] A. S. Fokas and M. J. Ablowitz, *The inverse scattering transform for the Benjamin–Ono equation: a pivot to multidimensional problems*, Stud. Appl. Math. **68** (1983), no. 1, 1–10. MR 84f:35139 Zbl 0505.76031

[19] G. Iooss, P. I. Plotnikov, and J. F. Toland, *Standing waves on an infinitely deep perfect fluid under gravity*, Arch. Ration. Mech. Anal. **177** (2005), no. 3, 367–478. MR 2007a:76017 Zbl 02222506

[20] D. J. Kaup and Y. Matsuno, *The inverse scattering transform for the Benjamin–Ono equation*, Stud. Appl. Math. **101** (1998), no. 1, 73–98. MR 2000e:34146 Zbl 1136.34349

[21] C. A. Kennedy and M. H. Carpenter, *Additive Runge–Kutta schemes for convection-diffusion-reaction equations*, Appl. Numer. Math. **44** (2003), no. 1-2, 139–181. MR 2003m:65111 Zbl 1013.65103

[22] R. J. LeVeque, *On the interaction of nearly equal solitons in the KdV equation*, SIAM J. Appl. Math. **47** (1987), no. 2, 254–262. MR 89c:35138 Zbl 0637.35078

[23] J. Marsden and A. Weinstein, *Reduction of symplectic manifolds with symmetry*, Rep. Mathematical Phys. **5** (1974), no. 1, 121–130. MR 53 #6633 Zbl 0327.58005

[24] Y. Matsuno, *Interaction of the Benjamin–Ono solitons*, J. Phys. A **13** (1980), no. 5, 1519–1536. MR 81d:35072 Zbl 0437.35062

[25] Y. Matsuno, *Note on the Bäcklund transformation of the Benjamin–Ono equation*, J. Phys. Soc. Japan **54** (1985), no. 1, 45–50. MR 86j:35140

[26] ______, *New representations of multiperiodic and multisoliton solutions for a class of non-local soliton equations*, J. Phys. Soc. Japan **73** (2004), no. 12, 3285–3293. MR 2005i:35237 Zbl 1066.35103

[27] K. R. Meyer, *Symmetries and integrals in mechanics*, Dynamical systems (Proc. Sympos., Univ. Bahia, Academic Press, New York, 1973, pp. 259–272. MR 48 #9760 Zbl 0293.58009

[28] A. Nakamura, *Bäcklund transform and conservation laws of the Benjamin–Ono equation*, J. Phys. Soc. Japan **47** (1979), no. 4, 1335–1340. MR 80m:35068

[29] J. Nocedal and S. J. Wright, *Numerical optimization*, Springer Series in Operations Research, Springer, New York, 1999. MR 2001b:90002 Zbl 0930.65067

[30] H. Ono, *Algebraic solitary waves in stratified fluids*, J. Phys. Soc. Japan **39** (1975), no. 4, 1082–1091. MR 53 #2129

[31] P. I. Plotnikov and J. F. Toland, *Nash–Moser theory for standing water waves*, Arch. Ration. Mech. Anal. **159** (2001), no. 1, 1–83. MR 2002k:76019 Zbl 1033.76005

[32] J. Satsuma and Y. Ishimori, *Periodic wave and rational soliton solutions of the Benjamin–Ono equation*, J. Phys. Soc. Japan **46** (1979), no. 2, 681–687.

[33] J. Stoer and R. Bulirsch, *Introduction to numerical analysis*, 3rd ed., Texts in Applied Mathematics, no. 12, Springer, New York, 2002. MR 2003d:65001 Zbl 1004.65001

[34] D. Viswanath, *Recurrent motions within plane Couette turbulence*, J. Fluid Mech. **580** (2007), 339–358. MR 2008f:76100 Zbl 05167861

[35] D. Viswanath, *The fractal property of the Lorenz attractor*, Phys. D **190** (2004), no. 1-2, 115–128. MR 2005a:37057 Zbl 1041.37013

[36] J. Wilkening, *An infinite branching hierarchy of time-periodic solutions of the Benjamin–Ono equation*, preprint, 2008. arXiv 0811.4209

[37] J. Wilkening, *An algorithm for computing Jordan chains and inverting analytic matrix functions*, Linear Algebra Appl. **427** (2007), no. 1, 6–25. MR 2008m:15034 Zbl 1132.47010

[38] J. Wilkening, *Math 228a: Numerical solution of differential equations*, lecture notes, 2007.

[39] C. Wulff, J. S. W. Lamb, and I. Melbourne, *Bifurcation from relative periodic solutions*, Ergodic Theory Dynam. Systems **21** (2001), no. 2, 605–635. MR 2002f:37088 Zbl 0986.37044

Received November 25, 2008. Revised July 12, 2009.

DAVID M. AMBROSE: ambrose@math.drexel.edu
Department of Mathematics, Drexel University, Philadelphia, PA 19104, United States

JON WILKENING: wilken@math.berkeley.edu
Department of Mathematics and Lawrence Berkeley National Laboratory, University of California, Berkeley, CA 94720, United States
http://math.berkeley.edu/~wilken